PCP
PLANT & CELL PHYSIOLOGY

Regular Paper

Tonoplast and Peroxisome Targeting of γ-tocopherol *N*-methyltransferase Homologs Involved in the Synthesis of Monoterpene Indole Alkaloids

Konstantinos Koudounas[1], Gregory Guirimand[1,2,†], Luisa Fernanda Rojas Hoyos[3], Ines Carqueijeiro[1], Pamela Lemos Cruz[1], Emily Stander[1], Natalja Kulagina[1], Jennifer Perrin[1], Audrey Oudin[1], Sébastien Besseau[1], Arnaud Lanoue[1], Lucia Atehortùa[4], Benoit St-Pierre[1], Nathalie Giglioli-Guivarc'h[1], Nicolas Papon[5], Sarah E. O'Connor[6] and Vincent Courdavault[1,*]

[1]EA2106 Biomolécules et Biotechnologies Végétales, Université de Tours, 31 Av. Monge, Tours 37200, France
[2]Graduate School of Sciences, Technology and Innovation, Kobe University, 1-1 Rokkodai, Nada, Kobe 657-8501, Japan
[3]Grupo de Biotransformación—Escuela de Microbiología, Universidad de Antioquia, Calle 70 No 52-21, A.A 1226, Medellín, Colombia
[4]Laboratorio de Biotecnología, Sede de Investigación Universitaria, Universidad de Antioquia, Medellin 50010, Colombia
[5]GEIHP, SFR ICAT, University of Angers, Université de Bretagne Occidentale, 4 rue de Larrey - F49933, Angers 49000, France
[6]Department of Natural Product Biosynthesis, Max Planck Institute for Chemical Ecology, Hans-Knöll-Straße 8, Jena 07745, Germany
[†]LE STUDIUM RESEARCH FELLOW, Loire Valley Institute for Advanced Studies.

*Corresponding author: E-mail, vincent.courdavault@univ-tours.fr

(Received 2 July 2021; Accepted 31 October 2021)

Many plant species from the Apocynaceae, Loganiaceae and Rubiaceae families evolved a specialized metabolism leading to the synthesis of a broad palette of monoterpene indole alkaloids (MIAs). These compounds are believed to constitute a cornerstone of the plant chemical arsenal but above all several MIAs display pharmacological properties that have been exploited for decades by humans to treat various diseases. It is established that MIAs are produced *in planta* due to complex biosynthetic pathways engaging a multitude of specialized enzymes but also a complex tissue and subcellular organization. In this context, *N*-methyltransferases (NMTs) represent an important family of enzymes indispensable for MIA biosynthesis but their characterization has always remained challenging. In particular, little is known about the subcellular localization of NMTs in MIA-producing plants. Here, we performed an extensive analysis on the subcellular localization of NMTs from four distinct medicinal plants but also experimentally validated that two putative NMTs from *Catharanthus roseus* exhibit NMT activity. Apart from providing unprecedented data regarding the targeting of these enzymes *in planta*, our results point out an additional layer of complexity to the subcellular organization of the MIA biosynthetic pathway by introducing tonoplast and peroxisome as new actors of the final steps of MIA biosynthesis.

Keywords: Alkaloids • *Catharanthus roseus* • *N*-methyltransferase • Peroxisome • Subcellular localization • Tonoplast

Introduction

Monoterpene indole alkaloids (MIAs) are plant specialized metabolites synthetized in thousands of plants from the Apocynaceae, Loganiaceae and Rubiaceae families (St-Pierre et al. 2013). Nowadays, more than 2,500 distinct MIAs have been described, which almost all derive from the common biosynthetic intermediate strictosidine (O'Connor and Maresh 2006). While their specific functions have not been firmly established to date, a growing number of evidences point out their involvement in responses of plants to environmental constraints and notably in defense processes to face bioagressor challenges (Dugé de Bernonville et al. 2017). Their high biological activities also confer to MIAs a prominent place in human pharmacopoeia with premium anticancer agents vinblastine and vincristine from the Madagascar periwinkle (*Catharanthus roseus*), the antimalarial quinine produced in the cinchona bark (*Cinchona officinalis*), the antiarrhythmic ajmaline synthesized by the devil pepper (*Rauwolfia serpentina*) or the nootropic vincamine accumulated in the dwarf periwinkle (*Vinca minor*) (O'Connor and Maresh 2006). Over the last decades, numerous studies established that MIAs are produced *in planta* thanks to complex routes encompassing up to 30–40 enzymatic steps in the aforementioned plants (Guirimand et al. 2010b, Courdavault et al. 2014, Caputi et al. 2018). These pathways involve enzymes from several protein families including P450, glucosyltransferases, β-glucosidases, dioxygenases, BAHD acyltransferases, decarboxylases, short- and medium-chain dehydrogenases/reductases,

Plant Cell Physiol. 63(2): 200–216 (2022) doi:https://doi.org/10.1093/pcp/pcab160, Advance Access publication on 10 November 2021, available online at https://academic.oup.com/pcp

'Pictet-Spenglerases' or *O*-methyltransferases and *N*-methyltransferases (NMTs) as non-exhaustive examples (Dugé de Bernonville et al. 2015a). Furthermore, these manifold reactions are accompanied by a complex organization of the MIA biosynthetic pathways *in planta* distributed in no less than four different cell types and six distinct subcellular compartments in *C. roseus* (Courdavault et al. 2014).

In this context, the quest for identification of new actors of these biosynthetic pathways has always remained challenging in the past decades for many research groups. This was particularly the case for the *S*-adenosyl-L-methionine (SAM)-dependent NMT involved in the biosynthesis of vindoline, a MIA specific to *C. roseus*. This enzyme, named 16-methoxy-2,3-dihydro-3-hydroxytabersonine *N*-methyltransferase (CrNMT), catalyzes the *N*-methylation of 16-methoxy-2,3-dihydro-3-hydroxytabersonine to desacetoxyvindoline in the biosynthesis of vindoline, one of the two precursors of vinblastine and vincristine (**Fig. 1**). While pioneering descriptions of this protein were published 30 years ago (De Luca et al. 1987, De Luca and Cutler 1987, Dethier and De Luca 1993), the corresponding gene was cloned nearly 20 years later (Liscombe et al. 2010). This elucidation was further accompanied by identifications of distinct NMTs involved in the synthesis of other MIAs in other medicinal plant species, including picrinine NMTs from both *V. minor* (VmPiNMT) and *R. serpentina* (RsPiNMT) yielding ervincine (**Fig. 1**) (Levac et al. 2016) but also norajmaline *N*-methyltransferase (RsNNMT) and ajmaline N_β-methyltransferase (RsANMT) from the ajmaline biosynthetic pathway in *R. serpentina* (**Fig. 1**) (Cázares-Flores et al. 2016). Importantly, phylogenetic analysis revealed that all these proteins originated from a common ancestor related to γ-tocopherol *C*-methyltransferase (γTMT), a broadly distributed enzyme catalyzing the formation of α-tocopherol within the vitamin E biosynthetic pathway. Accordingly, this phylogenetic relationship between all these plant NMTs gave rise to the so-called γ-tocopherol methyltransferase homolog group (γTMTh) (Liscombe et al. 2010, Cázares-Flores et al. 2016, Levac et al. 2016).

γ-Tocopherol methylation is common to all plants and was first characterized at the genetic level in Arabidopsis, cyanobacterium *Synechocystis* PCC6803 and pepper *Capsicum annuum*, revealing remarkable substrate specificities of γTMT, as observed later for MIA NMTs (Shintani and DellaPenna 1998, Koch et al. 2003). Interestingly, while the localization of the Arabidopsis γTMT (also referred to as VTE4) has been firmly established to be anchored in the plastid envelope membranes (Soll et al. 1985, Zbierzak et al. 2009), the subcellular localization of CrNMT still remains a matter of debate. Indeed, first cellular fractioning experiments associated CrNMT to the thylakoid membranes of chloroplasts (De Luca et al. 1987, De Luca and Cutler 1987, Dethier and De Luca 1993). However, analyses of the sequences predicted from cloned cDNAs failed to identify any chloroplast targeting peptide (cTP), leaving open the question of CrNMT subcellular localization (Liscombe et al. 2010, Cázares-Flores et al. 2016). Furthermore, with the exception of

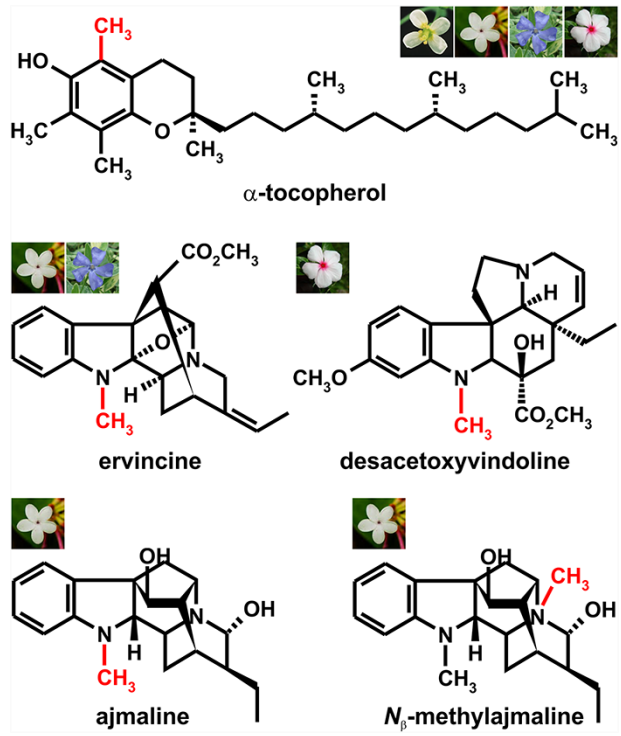

Fig. 1 Products resulting from *N*- or *C*-methyltransferase activities studied in this work. α-Tocopherol results from γ-tocopherol methylation by γTMT, ervincine from picrinine methylation by VmPiNMT or RsPiNMT, desacetoxyvindoline from 16-methoxy-2,3-dihydro-3-hydroxytabersonine methylation by CrNMT, ajmaline from norajmaline methylation by RsNNMT and N_β-methylajmaline by ajmaline methylation by RsANMT. The methyl group highlighted in red shows methylation position while flower pictures indicate methylated compound accumulation in *A. thaliana*, *R. serpentina*, *V. minor* and/or *C. roseus*.

dwarf periwinkle VmPiNMT that exhibits a potential secretory peptide, no other information regarding *Rauwolfia* RsPiNMT, RsANMT and RsNNMT localizations has been obtained to date. In opium poppy (*Papaver somniferum*), two NMTs involved in the biosynthesis of sanguinarine, namely, (*R*, *S*)-coclaurine *N*-methyltransferase (PsCNMT) and tetrahydroprotoberberine *N*-methyltransferase (PsTNMT), have been experimentally validated to be localized in the cytosol despite the existence of a potential tri-Lys (KKK) ER retention signal at the *C*-terminus (Hagel and Facchini 2012, Morris and Facchini 2019).

Overall, despite the importance of NMTs in the biosynthesis of numerous prominent alkaloids, little is known about the localization of these enzymes in plant cells. In this study, by expressing fusions with fluorescent proteins, we performed an extensive analysis of the subcellular localization of NMTs from four medicinal plants. Additionally, two previously unknown NMTs from *C. roseus* were found to catalyze *N*-methylation of picrinine, thus encoding functional NMTs *in planta*. Finally, beyond providing unprecedented information regarding NMT localization in plant cells, we added a new layer of complexity

to the subcellular organization of the MIA biosynthetic pathway by introducing tonoplast and peroxisome as new crucial compartments for the final steps of MIA synthesis.

Results

Identification of a putative C. roseus γTMT and prediction of γTMTh localizations

We first initiated this study by searching for an ortholog of the common ancestor of γTMThs in plants synthesizing MIAs to ensure that no divergence of γTMT localization occurs with previously published results (Zbierzak et al. 2009). The *C. roseus* CDF97 consensus transcriptome was thus screened by a BLAST analysis with VTE4 to identify the most similar transcript from periwinkle (SRR1144633_TR29246_c0_g1_i7_len = 1611; Dugé de Bernonville et al. 2015b). This sequence was further compared to the *C. roseus* genome to check for completeness and lack of other orthologs of high identity (Kellner et al. 2015). The protein deduced from the corresponding sequence (named hereafter putative *C. roseus* γTMT, pCrγTMT) exhibits an overall identity of 59% with VTE4 that reaches up to 71% without the highly divergent N-terminal end and includes the Rubisco large subunit methyltransferase motif regulating γTMT activity (Magnani et al. 2007) (**Supplementary Fig. S1**). Predictions of subcellular localizations performed using online bioinformatics predictors confirmed the presence of a putative cTP in the first 65 residues that could target this protein to plastids (**Fig. 2A, C**). The prediction was also applied to the five already cloned γTMThs. While this confirmed the previous identification of a putative secretory peptide at the N-terminal end of VmPiNMT (Levac et al. 2016) (**Fig. 2A, C**), no consensus in the prediction of its localization emerged from bioinformatics analyses that predicted targeting of protein to the endoplasmic reticulum (ER) or apoplast (**Fig. 2C**). A similar inconsistency was also obtained for RsPiNMT, RsANMT, RsNNMT and CrNMT, which were predicted to be located to peroxisomes, nucleus, cytosol or cytoskeleton although lacking any potential targeting sequences (**Fig. 2C**). For instance, prediction of RsNNMT and CrNMT to nucleus relies on the presence of weak monopartite nuclear localization sequences (NLS) (65-KKPR-68 in CrNMT) while possible targeting of RsPiNMT and RsANMT to peroxisomes mostly involve putative peroxisome targeting sequence type 1 (PTS1; 235-SRL-237 in RsANMT) located within the protein and are likely non-functional. Nevertheless, careful examination of γTMTh C-terminal extremities revealed the presence of a potential atypical PTS1 in CrNMT, according to previous studies (Reumann et al. 2016) (**Fig. 2B**). While this tripeptide (KSI) does not meet the exact atypical PTS1 definition, it includes one canonical (I) and two non canonical (KS) residues when two canonical and a single non-canonical residue are usually required. However and importantly, variations around PTS1 definition have been already described notably in *C. roseus* (Guirimand et al. 2012b). By contrast, C-terminal tripeptides of all other γTMThs only bear two canonical residues and are thus less prone to peroxisome targeting. In conclusion, all these discrepancies in the *in silico* prediction of localizations thus prompted us to experimentally investigate the subcellular localization of pCrγTMT and the five γTMThs involved in MIA biosynthesis.

The putative C. roseus γTMT is localized to membrane of plastid envelope

C. roseus cells are now well established as an appropriate host system for analyzing localization of MIA biosynthetic enzymes targeted to vacuoles (Guirimand et al. 2010a, Caputi et al. 2018, Carqueijeiro et al. 2018b), tonoplast (Payne et al. 2017) and plasma membrane (Héricourt et al. 2013), plastids (Guirimand et al. 2009, 2020, Thabet et al. 2012, Simkin et al. 2013), mitochondria (Guirimand et al. 2012a), ER (Besseau et al. 2013, Parage et al. 2016), nucleus (Stavrinides et al. 2015, 2016) and peroxisomes (Simkin et al. 2011, Guirimand et al. 2012b, Carqueijeiro et al. 2018a). On this basis, to compare localizations of AtγTMT (VTE4) and pCrγTMT, the VTE4 coding sequence was fused to YFP to express the VTE4-YFP fusion protein and to maintain cTP accessibility. By contrast, the pCrγTMT coding sequence was independently fused to both extremities of YFP to generate pCrγTMT-YFP and YFP-pCrγTMT to avoid masking of any other potential targeting peptide that would not have been identified by *in silico* prediction. After sequencing, each recombinant plasmid was co-transformed in *C. roseus* cells with plasmids expressing distinct subcellular compartment markers. In transiently transformed cells, pCrγTMT-YFP displayed a circular shaped fluorescence signal surrounding plastids (**Fig. 3A–H**). This signal did not overlap with the signal emitted by the CFP marker of the outer membrane of the plastid envelope, OEP7 (**Fig. 3I–L**) but perfectly merged with that of the marker of inner membrane of the plastid envelope, TIC40-CFP (**Fig. 3M–P**). Interestingly, VTE4-YFP displayed a similar distribution with circular shaped fluorescence signals co-localizing with the inner membrane of the plastid envelope (**Fig. 3Q–T**), strongly suggesting that it shares a similar localization with pCrγTMT-YFP. By contrast, the YFP-pCrγTMT exhibited a nucleocytosolic localization as confirmed by superimposition of the YFP fluorescent signal with that of the nucleocytosolic CFP marker (**Fig. 3U–X**), indicating that the N-terminal end of pCrγTMT must be accessible to drive this protein to plastids.

To further confirm that *C. roseus* cells are a suitable platform to study the subcellular localization of γTMThs from other species, we generated N- and C-termini fused YFP constructs of PsCNMT and PsTNMT from opium poppy. Transient co-expression of PsCNMT-YFP, YFP-PsCNMT, PsTNMT-YFP or YFP-PsTNMT constructs in *C. roseus* cells confirmed that the two NMTs exhibit a cytosolic localization since a perfect co-localization with the cytosolic marker (CFP-GUS) was observed (**Fig. 4**). As expected, these results are in agreement with previous subcellular localization studies of PsCNMT and PsTNMT in opium poppy cells (Hagel and Facchini 2012) and comfort the use of *C. roseus* cells for localization studies of heterologous enzymes.

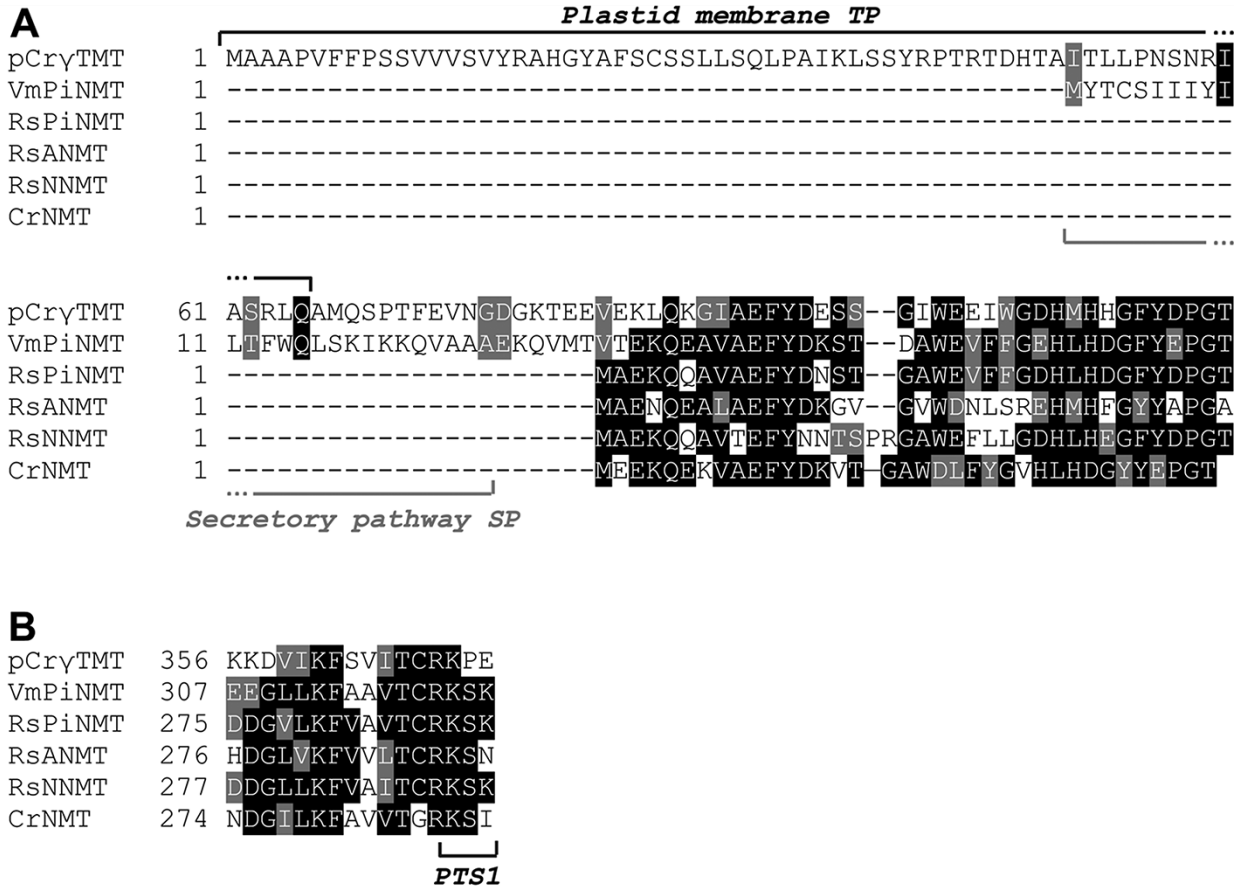

C

	PSORTII	WolfPSORT	ChloroP	TargetP	Predotar
pCrγTMT	OUT	PLAST	cTP (65AA)	cTP (65AA)	PLAST
VmPiNMT	ER	OUT	-	SP (25AA)	ER
RsPiNMT	PER	CYTO	-	-	ELSW
RsANMT	PER	CYSK	-	-	ELSW
RsNNMT	NUC	CYTO	-	-	ELSW
CrNMT	NUC	CYTO	-	-	ELSW

Fig. 2 Alignment of the N-terminal (A) and C-terminal (B) extremities of the putative pCrγTMT with the five γTMThs and prediction of localizations (C). Black lines highlight potential plastid targeting peptide (cTP) in pCrγTMT (A) and the putative peroxisome targeting signal type 1 (PTS1) in CrNMT (B) while gray line indicates a secretory pathway signal peptide (SP) in VmPiNMT (A). (C) Predictions were performed with the PSORTII, WolfPSORT and Predotar online predicators and identification of potential targeting sequences were achieved with TargetP and ChloroP. Only localization with the highest probability is shown as follow, CYTO, cytosol; CYSK, cytoskeleton; ELSW, elsewhere; NUC, nucleus; PER, peroxisome; PLAST, plastid; OUT, outside.

VmPiNMT and RsPiNMT exhibit differential subcellular localization

To initiate this comprehensive localization study of NMTs, we first investigated the subcellular targeting of VmPiNMT by creating YFP fusions at both N- and C- termini of VmPiNMT. Since TargetP predicted the existence of a signal peptide (sp) with a 54% likelihood at aa 23–27 (-VAAAE-), we also generated two truncated versions encompassing the first 30 (spVmPiNMT-YFP) or first 80 (sp2VmPiNMT-YFP) amino acids of VmPiNMT fused with YFP at the C-terminal. Transient co-expression of either VmPiNMT-YFP or YFP-VmPiNMT in *C. roseus* cells revealed that VmPiNMT perfectly co-localized with the cytosolic marker (CFP-GUS) (**Fig. 5A–H**). This localization was further validated in onion cells (i.e. a non-Apocynaceae species) in which VmPiNMT also resulted in cytosolic localization (**Fig. 5I–L**). Plasmolysis of cells showed

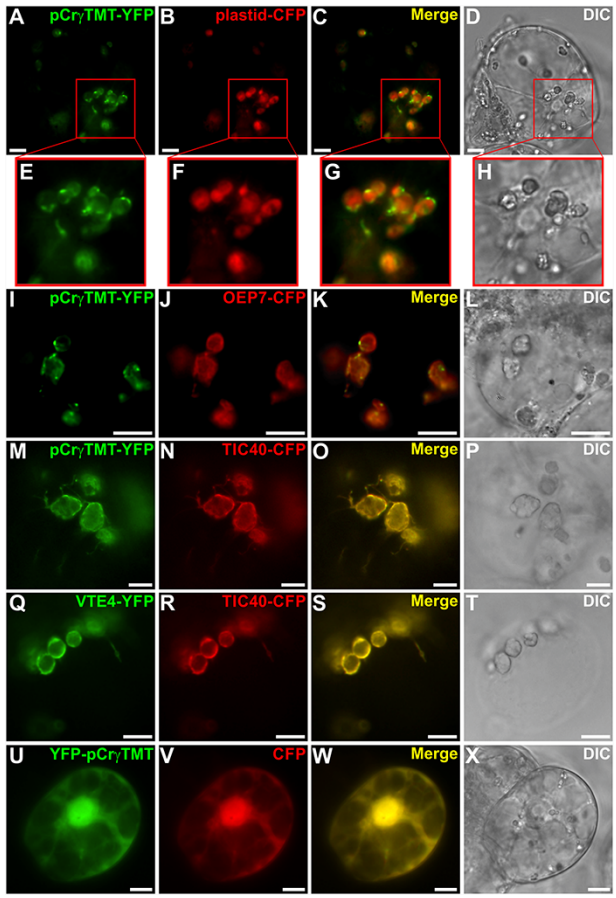

Fig. 3 pCrγTMT and VTE4-YFP are targeted to plastid envelop membrane. *C. roseus* cells were transiently co-transformed with plasmids expressing pCrγTMT (A, E, I, M, U) or VTE4-YFP (Q) and a plastid CFP marker (B, F), the marker of outer membrane of the plastid envelop OEP7-CFP (J), the marker of inner membrane of plastid envelop TIC40-CFP (N, R); or YFP-pCrγTMT (U) and a CFP nucleocytosolic marker (V). Co-localization of the two fluorescence signals appears on the merged images (C, G, K, O, S, W). Cell morphology (D, H, L, P, T, X) was observed with differential interference contrast (DIC). Bars, 10 μm.

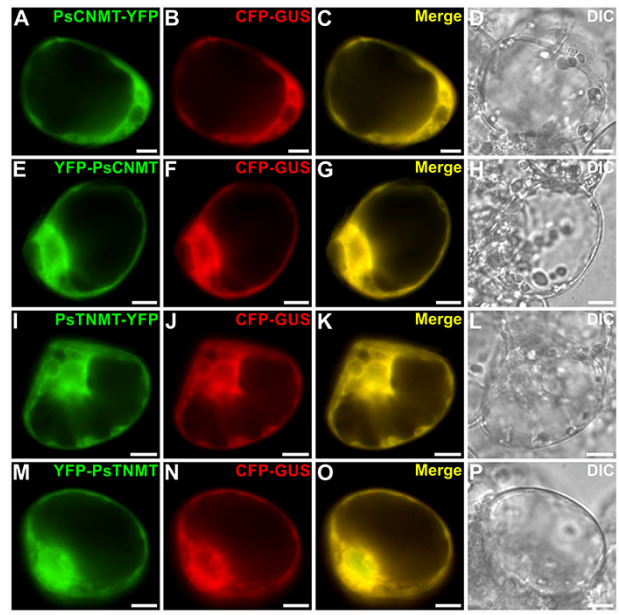

Fig. 4 Validation of the proper localization of PsCNMT and PsTNMT in *C. roseus* cells. *C. roseus* cells were transiently co-transformed with plasmids expressing PsCNMT-YFP (A) or YFP-PsCNMT (E) or PsTNMT-YFP (I) or YFP-PsTNMT (M) and a cytosolic marker (CFP-GUS; B, F, J and N). Co-localization of the two fluorescence signals appears on the merged images (C, G, K and O). Cell morphology (D, H, L and P) was observed with differential interference contrast (DIC). Bars, 10 μm.

that VmPiNMT remained in the cytosol thus confirming the lack of secretion (**Fig. 5M–N**). Additionally, both spVmPiNMT-YFP and sp2VmPiNMT-YFP constructs revealed a nucleocytosolic localization since the fluorescence signal was identical to the one from a nucleocytosolic CFP marker (**Fig. 5O–V**). Taken together, these results suggest that VmPiNMT does not encompass any signal peptide and is localized in the cytosol.

We next questioned whether the isoenzyme from *R. serpentina* (RsPiNMT) shares the same localization with VmPiNMT. Interestingly, transient expression of RsPiNMT-YFP in *C. roseus* cells revealed a potential tonoplastic-like localization, with fluorescence emanating from a large central vacuole (**Fig. 6A1–A2**) or from several small ones (**Fig. 6A3–A4**), which may also correspond to bulbs caused by YFP dimerization according to Segami et al. (2014). Such profiles of localization were also observed in onion cells, confirming that fusion protein targeting was independent from the cell type used for observations (**Fig. 6B1–C2**). However, many of our attempts to co-express RsPiNMT-YFP with a tonoplast marker (TPK-CFP) (Carqueijeiro et al. 2018b) resulted in the unexpected localization of both proteins and in the formation of aggregated foci during the first 24 h of observation (**Fig. 6D1–D4**). After longer incubations (36 h), a partial restoration of the tonoplastic localization was observed for both RsPiNMT-YFP and TPK-CFP thus suggesting that foci formation probably resulted from technical artifacts (**Fig. 6E1–E4**). Furthermore, co-transformation of RsPiNMT-YFP with a vacuolar marker (STR-CFP) allowed to confirm this tonoplastic localization as revealed by the YFP fluorescent signal enclosing that of the vacuole marker (**Fig. 6F1–F4**). In addition, expression of RsPiNMT N-terminally fused to YFP (YFP-RsPiNMT) revealed a cytosolic localization of the enzyme highlighted by the perfect co-localization with the cytosolic signal from the nucleocytosolic CFP marker and the loss of the tonoplastic targeting (**Fig. 6G1–G4**). This suggested that the N-terminal extremity of RsPiNMT needs to be accessible for proper localization of this enzyme. Surprisingly, the examination of the N-terminal amino acid sequence revealed that RsPiNMT does not encompass the typical tonoplastic targeting signal (D/E)$X_{3\text{-}5}$L(L/I) (Pedrazzini et al. 2013, Payne et al. 2017) or any other known tonoplast targeting peptide, and we were only able to identify a potentially atypical motif (133-DgtfdLV-139) in which the dibasic sequence encompasses a valine instead of a leucine or isoleucine residue. Taken together,

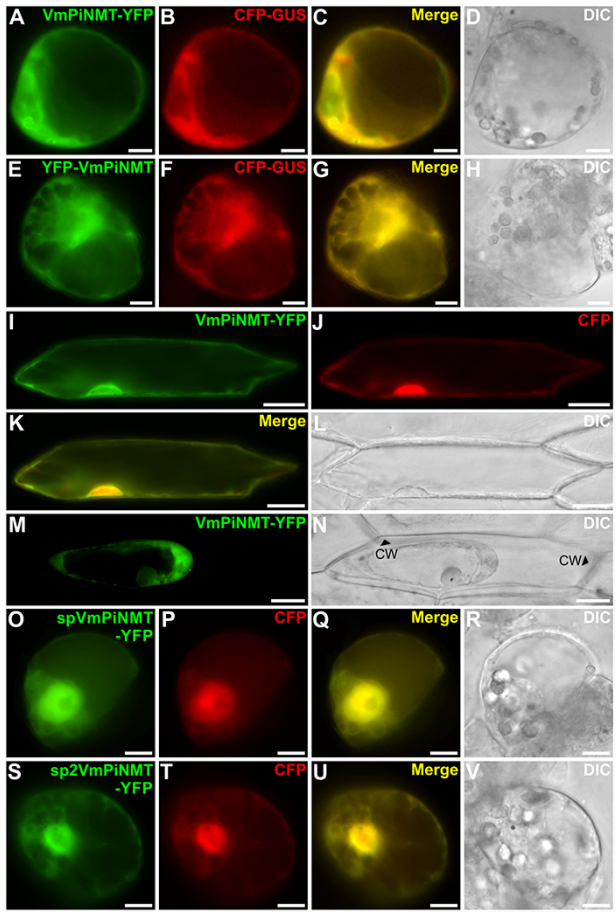

Fig. 5 VmPiNMT is localized in the cytosol. *C. roseus* cells (A-H, O-V) or onion cells (I-N) were transiently co-transformed with plasmids expressing VmPiNMT-YFP (A, I) or YFP-VmPiNMT (E) and a cytosolic marker (CFP-GUS; B, F,) or a nucleocytosolic marker (CFP; J). The plasmolysis of onion cells was performed to distinguish the signal from VmPiNMT-YFP and cell wall (CW, arrowheads). The existence of the predicted N-terminal signal peptide was tested by transiently co-transforming *C. roseus* cells with either spVmPiNMT-YFP (O) or tp2VmPiNMT-YFP (S) constructs and a nucleocytosolic CFP marker (P, T). Co-localization of the two fluorescence signals appears on the merged images (C, G, K, Q, U). Cell morphology (D, H, L, N, R, V) was observed with differential interference contrast (DIC). Bars, 10 μm (A–H, M–T) and 100 μm (I–N).

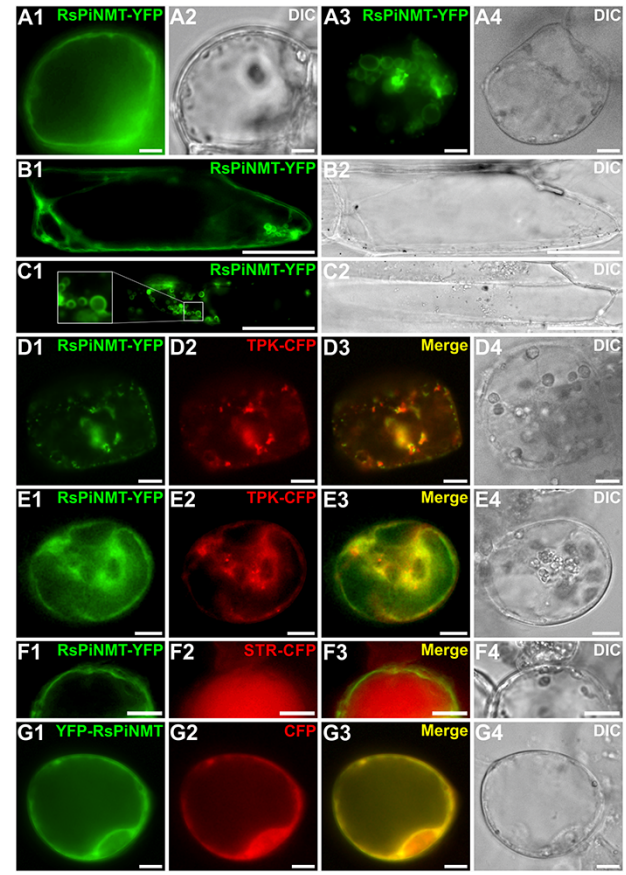

Fig. 6 RsPiNMT exhibits a tonoplast-like localization. *C. roseus* cells (A1, A3, D1, E1, F1 and G1) or onion cells (B1, C1) were transiently transformed with a plasmid expressing RsPiNMT-YFP (A1, A3, B1, C1), co-transformed with plasmids expressing either RsPiNMT-YFP and the tonoplastic marker (TPK-CFP; D2, E2) or the vacuolar marker (STR-CFP; F2); or YFP-RsPiNMT (G1) and a nuclocytosolic CFP marker (G2). Co-localization of the two fluorescence signals appears on the merged images (D3,E3,F3 and-G3). Cell morphology (A2, A4, B2, C2, D4, E4, F4 and G4) was observed with differential interference contrast (DIC). Bars, 10 μm (A1–A4, D1–G4) and 100 μm (B1–C2).

these results suggest that RsPiNMT displays a tonoplast localization via a—yet to be characterized—non-canonical N-terminal sequence.

RsNNMT and RsANMT exhibit a pre-vacuolar compartment-arrested localization

To gain more insight into the subcellular localizations of NMTs, additional localizations of enzymes from *R. serpentina* were achieved notably for RsNNMT and RsANMT from the ajmaline biosynthetic branch specific to *Rauwolfia sp*. Interestingly, the expression of RsNNMT and RsANMT fused to the N-terminal end of YFP (Rs-NNMT-YFP, RsANMT-YFP) revealed a punctuated pattern of fluorescence in *C. roseus* cells, but distinct from the one observed for RsPiNMT (**Fig. 7A–D**). Accordingly, such a pattern was also observed in onion cells for RsNNMT-YFP (**Fig. 7E–F**). However, we noticed that the fluorescence foci observed for RsNNMT-YFP and RsANMT-YFP perfectly superimposed with the signal emitted by pre-vacuolar compartment (PVC) marker RFP-VSR2 (Shen et al. 2013) (**Fig. 7G–J, O–R**). By contrast, expressing RsNNMT and RsANNMT fused with YFP in the opposite orientation (YFP-RsNNMT and YFP-RsANMT) led to the loss of this punctuated signal and resulted in a cytosolic localization as revealed by co-transforming the cells with the cytosolic marker (CFP-GUS) (**Fig. 7K–N, S–V**). Overall, these results thus suggest that RsNNMT and RsANMT contains an active targeting signal at their N-terminus thus suggesting localization of the native proteins in PVCs. However, it is worth

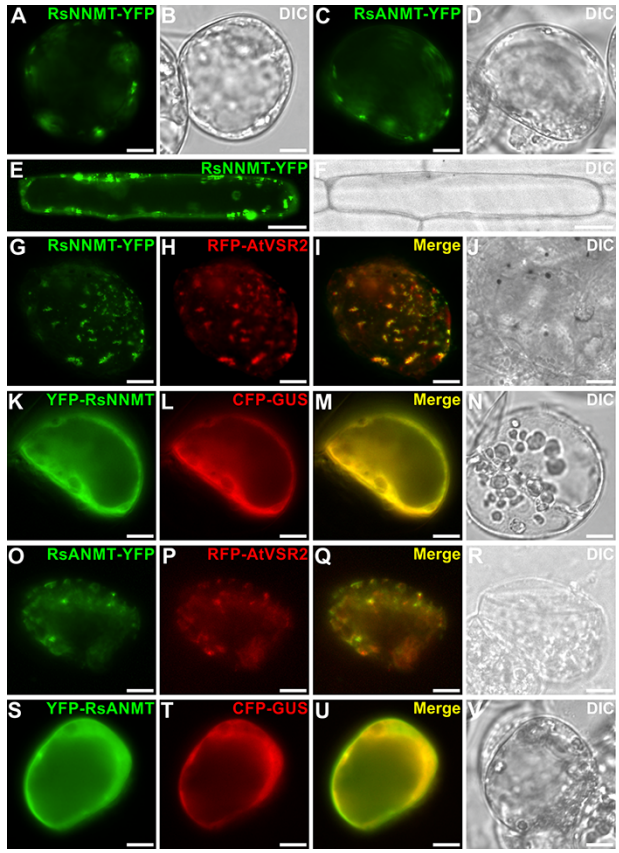

Fig. 7 RsNNMT and RsANMT exhibit a PVC-arrested localization. *C. roseus* cells (A–D, G–V) and onion cells (E–F) were transiently co-transformed with a plasmid expressing either RsNNMT-YFP (A–B; E–J), or RsANMT (C–D; O–R) or YFP-RsNNMT (K–N) or YFP-RsANMT (S–V) and either with the pre-vacuolar compartment (PVC) marker (RFP-VSR2; G–J; O–R) or the cytosolic marker (CFP-GUS; K–N; S–V) or without a marker (A–F). Co-localization of the two fluorescence signals appears on the merged images (I, M, Q, U). Cell morphology (B, D, F, J, N, R, V) was observed with differential interference contrast (DIC). Bars, 10 μm (A–D, G–V) and 100 μm (E–F).

noting that while PVC-arrested localizations were observed for both fusion proteins, no definitive vacuolar/tonoplast targeting was observed after prolonged observation as described for RsPiNMT.

CrNMT is targeted to peroxisomes in *C. roseus* cells

Since studies on NMTs subcellular localization revealed heterogeneous results—even among isoenzymes from different species (i.e. VmPiNMT and RsPiNMT), we next performed a more detailed analysis of the γTMThs homologs from *C. roseus*. Although CrNMT is well known to be engaged in the biosynthetic pathway of vindoline (De Luca et al. 1987, De Luca and Cutler 1987, Dethier and De Luca 1993, Liscombe et al. 2010), the subcellular localization of this enzyme has not been explored by direct methodologies (i.e. microscopic analysis of YFP-fused constructs) and the predicted plastid/thylakoid localization was only based on cell fractionation in sucrose gradient (De Luca and Cutler 1987, Dethier and De Luca 1993). Therefore, to further characterize the localization of this enzyme, we created fusions between CrNMT and the N- or C-terminal end of YFP (CrNMT-YFP and YFP-CrNMT) for transient expression in *C. roseus* cells. Expressing CrNMT-YFP together with a nucleo-cytoplasmic marker (CFP) suggested a nucleocytosolic localization of CrNMT-YFP as revealed by the perfect superimposition of the two fluorescence signals (**Fig. 8A1–A4**). By contrast, the inverted construct (YFP-CrNMT), displaying an accessible CrNMT C-terminal end, exhibited a more complex localization (**Fig. 8B1–B4**). While a substantial part of the fluorescence signal emerged from the cytosol, more discrete fluorescent punctuations detached from the cytosolic signal were also observed (**Fig. 8B1–B4**). Interestingly, co-transformation of the YFP-CrNMT expressing plasmid with the plasmid encoding the peroxisome CFP marker (perox-CFP) show a partially similar pattern of fluorescence and a perfect merging of the fluorescence signal emitted by punctuations (**Fig. 8C1–C4**). Besides showing that PSORTII and WolfPSORT predictions were not accurate as for most of the NMT studied in this work (**Fig. 2C**), this result suggested that CrNMT was at least partially targeted to peroxisomes in agreement with the potential presence of a non-canonical PTS1 (**Fig. 2B**).

To gain insight into this particular localization, additional transformations were performed and accompanied by cell treatments by cycloheximide. By inhibiting translation of newly produced fluorescent proteins, this treatment was shown to efficiently improve detection of peroxisomes in transiently transformed cells through limiting the overflow of the peroxisome import machinery and allowing peroxisome targeting of the remaining already produced fusion proteins (Guirimand et al. 2012b). Indeed, while YFP-CrNMT exhibited a similar mixed localization in both peroxisomes and cytosol at the beginning of the cycloheximide treatment (**Fig. 8D1–D4**), a complete targeting to peroxisomes was observed after 4 h, suggesting that peroxisomes may represent the exclusive destination of CrNMT (**Fig. 8E1–F4**). Closer observations highlighted the entire superimposition of the YFP-CrNMT fluorescence signal with that of the peroxisomal-CFP marker targeted to peroxisome lumen suggesting that CrNMT is rather located to this peroxisomal compartment. In addition, we also generated a truncated version of CrNMT deleted of the C-terminal PTS1 and at the C-terminal end of YFP (YFP-CrNMTΔ). Interestingly, this fusion protein totally lost the targeting to peroxisomes and only exhibited a nucleo-cytoplasmic localization (**Fig. 8G1–G4**). This last result combined to previous ones strongly suggest that CrNMT is targeted at least partially to peroxisomes through a C-terminal tripeptide (-KSI) corresponding to a non-canonical PTS1 signal that is necessary for proper localization *in planta*.

Subcellular organization of other *C. roseus* γTMThs and validation of their *N*-methyltransferase activity

The unexpected localization of CrNMT prompted us to study the localization of other γTMThs closely related to pCrγTMT.

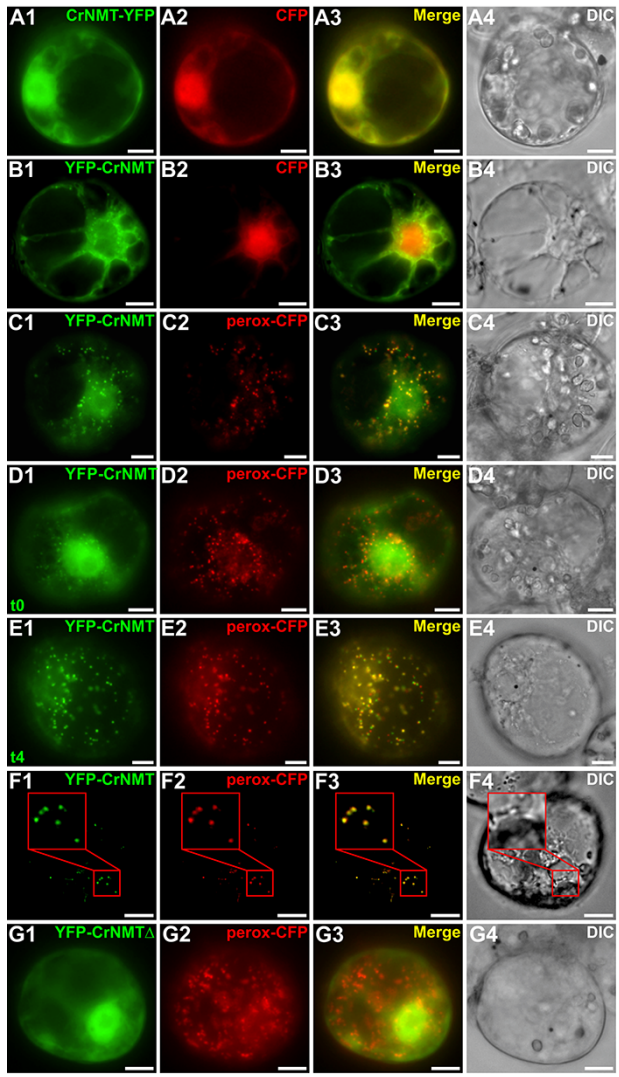

Fig. 8 CrNMT is localized in the peroxisomes. *C. roseus* cells were transiently co-transformed with a plasmid expressing either CrNMT-YFP (A1) or YFP-CrNMT (B1-F1) or YFP-CrNMTΔ (G1) and either the nucleocytosolic marker (CFP; A2 and B2) or the peroxisome marker (perox-CFP; C2–G2). To enhance peroxisome visualization, cells were cultivated 14 h prior harvesting and treatment with 2 μM cycloheximide. Cells were observed immediately (*t*0, D1) or 4 h (*t*4, E1) after treatment. A magnification of the signal emitted by YFP-CrNMT and the perox-CFP marker is presented in F1–F4. Co-localization of the two fluorescence signals appears on the merged images (A3–G3). Cell morphology (A4–G4) was observed with differential interference contrast (DIC). Bars, 10 μm.

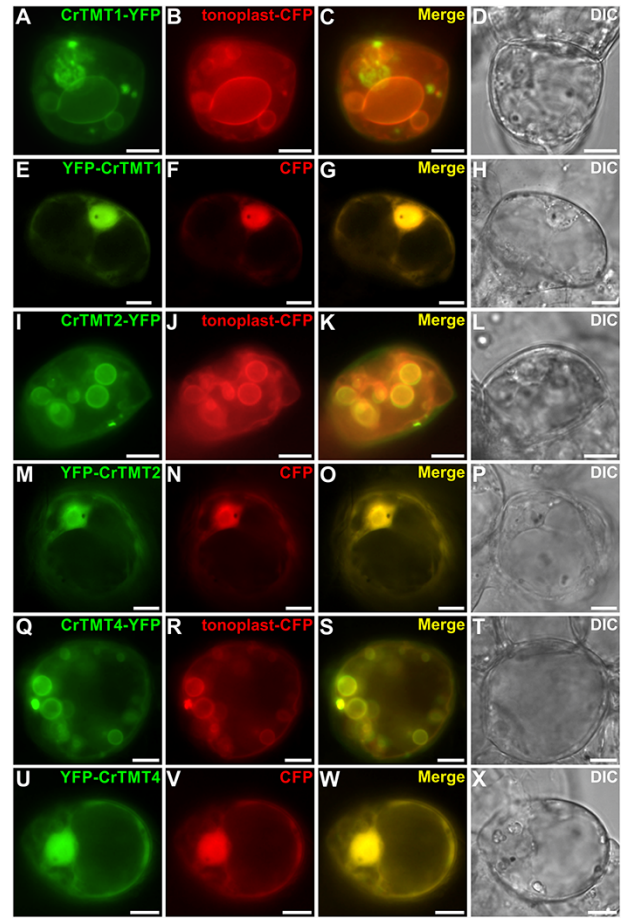

Fig. 9 The three *C. roseus* γTMThs (TMT1, TMT2, TMT4) are targeted to the tonoplast. *C. roseus* cells were transiently co-transformed with a plasmid expressing either CrTMT1-YFP (A–D) or CrTMT2-YFP (I–L) or CrTMT4-YFP (Q–T) or YFP-CrTMT1 (E-H), YFP-CrTMT2 (M–P) YFP-CrTMT4 (U–X) and either the tonoplast marker (TPK-CFP; B, J, R) or the nucleocytosolic marker (CFP; F, N, V). Co-localization of the two fluorescence signals appears on the merged images (C, G, K, O, S, W). Cell morphology (D, H, L, P, T, X) was observed with differential interference contrast (DIC). Bars, 10 μm.

Blasting the *C. roseus* transcriptome and genome allowed to identify three additional candidates namely CRO_113801 (CrTMT1) and the two previously reported CRO_111268 (CrTMT2) and CRO_11267 (CrTMT4) identified as Cr3710017 and Cr7756 by (Liscombe et al. 2010) (**Supplementary Figs. S2 and S3A**). All the corresponding genes were expressed in leaves, flowers and roots (**Supplementary Fig. S3B**). For localization studies, the three corresponding proteins were thus transiently expressed in *C. roseus* cells as fusions with either the N- or C-terminal end of YFP (**Fig. 9A–X**). Interestingly, on most of the observed cells, all the three γTMThs fused to the N-terminal end of YFP (CrTMT1-YFP, CrTMT2-YFP, CrTMT4-YFP) exhibited a fluorescence profile perfectly merging with that of the tonoplast marker (TPK-CFP) 24 h after transformation, with also potential bulbs (**Fig. 9A–D**, **I–L**, **Q–T**). By contrast, the constructs fused with YFP in the inverted orientation (YFP-CrTMT1, YFP-CrTMT2, YFP-CrTMT4) were not targeted to the tonoplast as revealed by the superimposition of fluorescence signal with the nucleocytosolic marker (CFP; **Fig. 9E–H**, M–P, U–X). All these results thus suggested that CrTMT1, CrTMT2 and CrTMT4 are targeted to the tonoplast as previously observed for RsPiNMT (**Fig. 6**). However, it is worth noting that none of the three γTMThs displays the consensus tonoplast targeting signal (D/E)$X_{3\text{-}5}$L(L/I) (Pedrazzini et al. 2013, Payne et al. 2017,

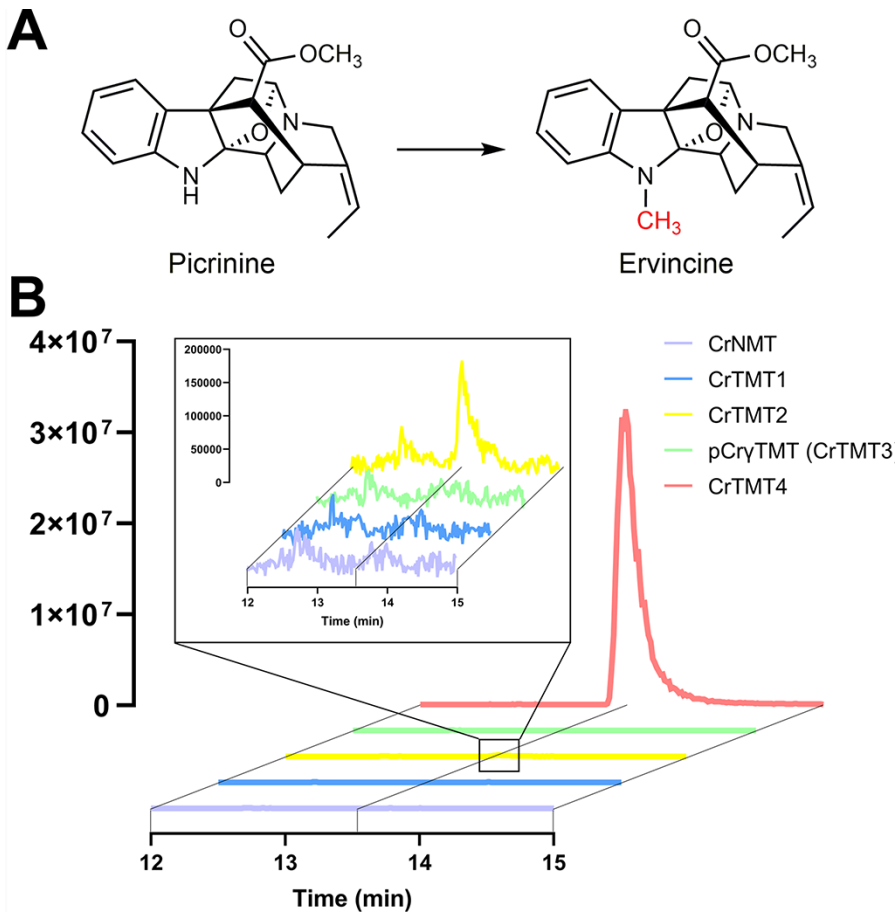

Fig. 10 *In vitro* enzymatic assays of recombinant CrTMTs against picrinine. (A) The chemical structures of picrinine (substrate) and ervincine (product). (B) UPLC-MS chromatograms at *m*/*z* 353 among enzymatic assays. Ervincine production was screened after incubating the respective purified recombinant proteins with picrinine. *Y*-axis corresponds to AU. A new peak at the *m*/*z* corresponding to *N*-methylated picrinine was detected only in the case of CrTMT4 and CrTMT2 (depicted in the inset).

Wojcik and Kriechbaumer 2021) and no closely related pattern could be identified within their N-terminal region.

To get more insight into the potential functions of these three additional γTMThs, we analyzed the genomic organization of the corresponding genes in the recently released draft genome of *C. roseus* (Franke et al. 2019). Interestingly, while *CrTMT1* (CRO_113801) and *pCrγTMT* (*CrTMT3*;CRO_130556) are distributed on two distinct scaffolds (cro_v2_scaffold_186 and cro_v2_scaffold_51, respectively), *CrTMT2* (CRO_111268) and *CrTMT4* (CRO_111267) are located in the same genomic region (cro_v2_scaffold_163) and in close proximity with *CrNMT* (CRO_111273) (**Supplementary Fig. S4**). This genomic organization thus suggests that *CrTMT2*, *CrTMT4* and *CrNMT* may originate from local gene duplication and possibly encode related enzymes. To investigate whether the putative γTMThs from *C. roseus* encode for functional NMTs, we generated recombinant enzymes in *E. coli* (**Supplementary Fig. S5**) and performed *in vitro* enzymatic assays. Given the sequence identity and similarity of localization between CrTMT2, CrTMT4 and RsPiNMT, *in vitro* assays were conducted with picrinine as a substrate to potentially produce ervincine (**Fig. 10A**). As expected, the γ-tocopherol *C*-methyltransferase pCrγTMT (CRO_130556) did not exhibit any *N*-methylation activity (**Fig. 10B**). In addition, no *N*-methylated product was observed when CrNMT (CRO_111273) or CrTMT1 (CRO_113801) was incubated with picrinine. By contrast, incubation of CrTMT2 (CRO_111268) or CrTMT4 (CRO_111267) with picrinine, resulted in a new peak at *m*/*z* 353 indicative of a potential conversion of picrinine into ervincine (*N*-methylpicrinine). The conversion was more than 100 times higher with CrTMT4 compared to CrTMT2. These results thus showed that both CrTMT2 and CrTMT4 exhibit alkaloid NMT activity and supported a potential evolutionary relationship with CrNMT.

Discussion

Numerous species from the Apocynaceae family produce MIAs that display high biological activities (O'Connor and Maresh 2006). Among the enzymes engaged in the corresponding biosynthetic pathways, alkaloid NMTs constitute a recently described subgroup of γTMThs, also involved in the synthesis of other alkaloid types such as benzylisoquinoline alkaloids

(BIAs) for instance (Liscombe et al. 2010, Cázares-Flores et al. 2016, Levac et al. 2016). Despite pioneering studies aiming at functionally characterizing alkaloid NMTs, little is known hitherto about their subcellular localization. Previous subcellular localization studies of alkaloid NMTs performed by direct methodologies (e.g. microscopic observation of fluorescent protein (FP)-fused chimeric constructs) have been limited to a few species including opium poppy and the coffee (*Coffea arabica*) and all revealed a cytoplasmic distribution of these enzymes (Kodama et al. 2008, Hagel and Facchini 2012). The cytoplasmic localization seems to be basically a common feature of methyltransferases since also reported for alkaloid *O*-methyltransferases involved in the biosynthesis of the BIA sanguinarine like (*R,S*)-3′-hydroxy-*N*-methylcoclaurine 4′-*O*-methyltransferase (4′OMT) and (*R,S*)-norcoclaurine 6-*O*-methyltransferase (6OMT) (Hagel and Facchini 2012) or the synthesis of vindoline (16 hydroxytabersonine 16-*O*-methyltransferase, 16OMT) (Guirimand et al. 2011b). Furthermore, other *O*-methyltransferases involved in iridoid, phenylpropanoid/flavonoid or anthocyanin/flavonol biosynthesis have been also located to cytoplasm (Hugueney et al. 2009, Guirimand et al. 2011a, Shaipulah et al. 2016). However, besides this cytoplasmic localization, plastids are known to host other methyltransferases such as the γTMT engaged in γ-tocopherol methylation (Zbierzak et al. 2009). In addition, *N-*, *O-* or *S*-methyltransferases not directly related to specialized metabolisms are also located to the nucleus (Choi et al. 2014), the ER membrane (Bracha-Drori et al. 2008), the Golgi apparatus (Lee et al. 2012) and the chloroplast (Ravanel et al. 2004, Tamiru et al. 2016). Therefore, the apparent highly diverse distribution of methyltransferases prompted us at deepening the study of their subcellular localization by notably focusing on NMTs involved in MIA synthesis.

We validated the use of *C. roseus* cells as a suitable platform for subcellular localization studies by confirming the localization of already characterized *C*-methyltransferases or NMTs. For instance, Arabidopsis AtγTMT (VTE4) correctly targeted the plastid membranes (**Fig. 3**) and the two opium poppy *N*-methyltransferases (PsTNMT and PsCNMT) in the cytosol, as previously reported (**Fig. 4**) (Zbierzak et al. 2009, Hagel and Facchini 2012). We also showed that the *C. roseus* homolog of AtγTMT (pCrγTMT, CrTMT3) was located on the inner membrane of the plastid envelope in agreement with its putative role in vitamin E synthesis (Muñoz and Munné-Bosch 2019) (**Fig. 3**).

Based on this system, we next highlighted differences of localization between two orthologues of PiNMT. In contrast to *in silico* predictions (**Fig. 2C**), we first described cytosolic localization of VmPiNMT invalidating the prediction of a potential targeting peptide at the N-terminal end (**Fig. 5**). This result was further confirmed in onion cells as well as with two truncated constructs bearing the first 30 or 80 amino acids fused in frame with YFP. Such a cytoplasmic localization is consistent with the distribution of PsTNMT, PsCNMT and NMTs involved in caffeine biosynthesis (Kodama et al. 2008). It also matches with the cytoplasmic localization of many other MIA biosynthetic enzymes such as tryptophan decarboxylase, iridoid synthase, 7-deoxyloganetic acid glucosyltransferase, loganic acid *O*-methyltransferase as well as desacetoxyvindoline 4-hydroxylase and deacetylvindoline 4-*O*-acetyltransferase (Miettinen et al. 2014, Dugé de Bernonville et al. 2015a) making of the cytosol a common crossroad for MIA production. However, we secondly showed that the ortholog from *R. serpentina* (RsPiNMT) that is devoid of any predicted targeting peptide displayed unexpected tonoplast localization (**Fig. 6**). Although not common, differences in ortholog localization has been already reported for the NMT theobromine synthase that exhibits distinct subcellular targeting among *C. arabica* and *Camellia gymnogyna* (Kodama et al. 2008, Teng et al. 2020). Different localization of RsPiNMT and VmPiNMT may thus point out to a differential compartmentalization for a similar reaction among the Rauvolfiinae and Vincinae subtribes. Interestingly, apart from RsPiNMT, we also showed that the three γTMThs identified in *C. roseus* (CrTMT1, CrTMT2 and CrTMT4) also exhibited a tonoplast localization when their N-terminal end was accessible (**Fig. 9**). These localizations suggest that the tonoplast localization may be observed for different methyltransferases as also previously suggested by proteomic approaches of tonoplast-enriched fractions for methyltransferase homologues (Endler et al. 2006, Shen et al. 2014). Although not common, other examples of specialized metabolisms have been associated with the tonoplast by direct methodologies such as enzymes involved in flavonoid biosynthesis (Saslowsky and Winkel-Shirley 2001, Toda et al. 2012). However, this tonoplast localization raised some important questions about the corresponding targeting mechanisms and membrane anchoring processes. Regarding targeting, we first noted that the tonoplast localization was disrupted when YFP was fused to the N-terminal of the enzymes since a nucleocytosolic localization was observed, thus confirming that N-terminal accessibility of RsPiNMT, CrTMT1, CrTMT2 and CrTMT4 is critical for a proper localization. In plants, localization of proteins to the tonoplast has been associated to the targeting signal $(D/E)_{X3\text{-}5}L(L/I)$ (Pedrazzini et al. 2013, Payne et al. 2017, Wojcik and Kriechbaumer 2021). However, no closely related motif could be identified in the N-terminal amino acid sequences of the four enzymes, except a potentially atypical motif in RsPiNMT. This still lets open the question of how these methyltransferases are targeted to the tonoplast but the lack of clearly identifiable sequences seems to be not prohibitive since two calcium sensors from Arabidopsis (CBL2 and CBL3) are known to be localized in the tonoplast *via* N-terminal domains while not exhibiting any known tonoplast targeting signal (Tang et al. 2012).

Regarding tonoplast anchoring, no evident potential transmembrane helices could be predicted in the primary sequences of RsPiNMT, CrTMT1, CrTMT2 and CrTMT4 albeit some discrepancies exist between the MemBrain and TMHMM servers (**Supplementary Table S2**). Similarly, no known post-translational protein modification involved in membrane anchoring could be identified with a high confidence

(**Supplementary Table S3**). This outcome resembles the Arabidopsis VTE4 and its rice homologue that are located to the inner membrane of the plastid envelope without any identified transmembrane domains (Bréhélin et al. 2007, Zbierzak et al. 2009, Jo and Hyun 2011). In addition, it should be noted that the characterization of interactions among flavonoid biosynthetic enzymes assembling in varying metabolons suggested that the observed localizations could be due to interactions between proteins (Nakayama et al. 2019). Such a mechanism could thus be also considered for tonoplast association of alkaloid NMTs. Besides this mechanistic consideration, the tonoplast targeting of RsPiNMT, CrTMT1, CrTMT2 and CrTMT4 also questioned about possible roles in MIA synthesis. Interestingly, the anabolism of some MIA precursors in *C. roseus* is known to depend on several trans-tonoplast translocations of intermediates (Guirimand et al. 2011a) and at least two enzymes involved in MIAs biosynthesis (i.e. STR; strictosidine synthase and PRX1; peroxidase 1) are known to be localized in vacuoles where strictosidine synthesis occurs (Costa et al. 2008, Guirimand et al. 2010a). It is thus possible to hypothesize that the tonoplast localization of alkaloid NMTs would favor the methylation reaction of MIAs that are ultimately stored in the vacuole. Interestingly, we also showed that both RsNNMT and RsANMT exhibited a PVC localization since the corresponding YFP-fused proteins co-localized with the PVC marker RFP-VSR2 (Shen et al. 2013) (**Fig. 7**). However, numerous observations suggested that the localization was PVC-arrested since no ultimate vacuolar targeting was observed. This is thus slightly different from the precondylocarpine acetate synthase which is progressively secreted to the vacuole by ER-derived vesicles (Caputi et al. 2018). This is also different from other enzymes that reach the tonoplast through PVCs as illustrated for AtβFructosidase 4 (Jung et al. 2011). On the other hand, this result is in agreement with older observations that associated enzymes involved in MIAs precursor biosynthesis with vesicles in *C. roseus* (Madyastha et al. 1977) as well as for columbamine-*O*-methyltransferase (Rueffer et al. 1986), stilbene synthase (Fornara et al. 2008) and nicotianamine synthase (Nozoye et al. 2014).

While the 16-methoxy-2,3-dihydro-3-hydroxytabersonine-*N*-methyltransferase activity has been described more than 30 years ago in *C. roseus* and the corresponding enzyme identified more recently (De Luca et al. 1987, De Luca and Cutler 1987, Dethier and De Luca 1993, Liscombe et al. 2010), the subcellular localization of CrNMT has still remained a matter of debate. In this work, we showed that CrNMT is at least partially targeted to peroxisomes via a non-canonical PTS1 (**Figs. 2B**, **8**). Most of the proteins targeted to peroxisomes encompass a PTS1 tripeptide at their extreme C-terminal end, which mostly correspond to the canonical consensus [SA][RK][LMI] sequences (Reumann et al. 2016). However, several studies have validated that various combinations of tripeptides encode for functional but non-canonical PTS1s such as the [SAPCFVGTLKIQ][RKSNLMHGETFPQCYDA][LMIVYF] sequences (Reumann et al. 2016). The putative non-canonical PTS1 (-KSI) at the C-terminal of CrNMT falls within the reported range of residues that constitute the non-canonical PTS1 tripeptides. This has been experimentally validated by deletion of this tripeptide which resulted in the loss of the peroxisome targeting of YFP-CrNMTΔ (**Fig. 8**). While CrNMT has been originally associated to the thylakoid membranes of chloroplasts by subcellular fractionation (De Luca et al. 1987, De Luca and Cutler 1987, Dethier and De Luca 1993), no plastid targeting sequences has been identified after identification of the corresponding gene (Liscombe et al. 2010). The previously reported plastid localization may thus be due to the initial experimental procedure used for enzyme characterization since peroxisomes are known to sediment similarly to chloroplasts (Abas and Luschnig 2010) resulting in cross organellar contamination in isolated fractions (Eubel et al. 2007). From a physiological point of view, the targeting of CrNMT to peroxisomes reinforces the involvement of this subcellular compartment in the biosynthesis of MIAs since it also hosts enzymes involved in the synthesis of the monoterpenoid precursor of MIAs (Simkin et al. 2011, Thabet et al. 2011, Guirimand et al. 2012a). In addition, other enzymes involved in alkaloid synthesis have been previously reported to be localized in peroxisomes such as the *N*-methylputrescine oxidase and its close homolog NtDAO1 engaged in nicotine biosynthesis in tobacco (Naconsie et al. 2014). To date, Arabidopsis HARMLESS TO OZONE LAYER 3 (AT2G43940) is the only example of a plant methyltransferase known to be localized in peroxisomes, although the *in planta* function of this enzyme remains unknown (Pan et al. 2018). Interestingly, COBALAMIN-INDEPENDENT METHIONINE SYNTHASE1 (ATMS1 or METS1; AT5G17920) an enzyme involved in the production of SAM—the universal donor of most methyltransferases—was also identified as a peroxisomal by N-terminal FP fused constructs confirming the capacity of methyltransferases to function in this compartment (Quan et al. 2013, González and Vera 2019). Other transferases (EC: 2.-) involved in primary metabolism that exhibit a peroxisomal localization include acyltransferases (Pracharoenwattana et al. 2005, Carrie et al. 2007, Tanabe et al. 2011), an aminotransferase (ASP3; At5g11520) (Eubel et al. 2008) and glutathione S-transferase T1 (GSTT1; At5g41210) (Reumann et al. 2007) supporting the idea that peroxisome is a hub for many metabolic pathways. In the tabersonine to vindoline pathway, while all other reactions occur in the cytosol, even for the ER-anchored P450, the peroxisomal targeting of CrNMT may constitute a regulatory step in this biosynthetic branch, besides adding a new layer of complexity to the architecture of the MIA biosynthetic pathway (**Fig. 11**).

Finally, the analysis of the genomic organization encompassing CrNMT showed that CrTMT2 and CrTMT4 are clustered in close proximity with CrNMT suggesting they may be functionally related genes (Nützmann et al. 2016). Physically clustered homologs most likely result from tandem gene duplication events and the expanded gene pools can potentially give rise to sub- or neo-functionalization due to absence of selective pressure on the new copies (Moore and Purugganan 2005,

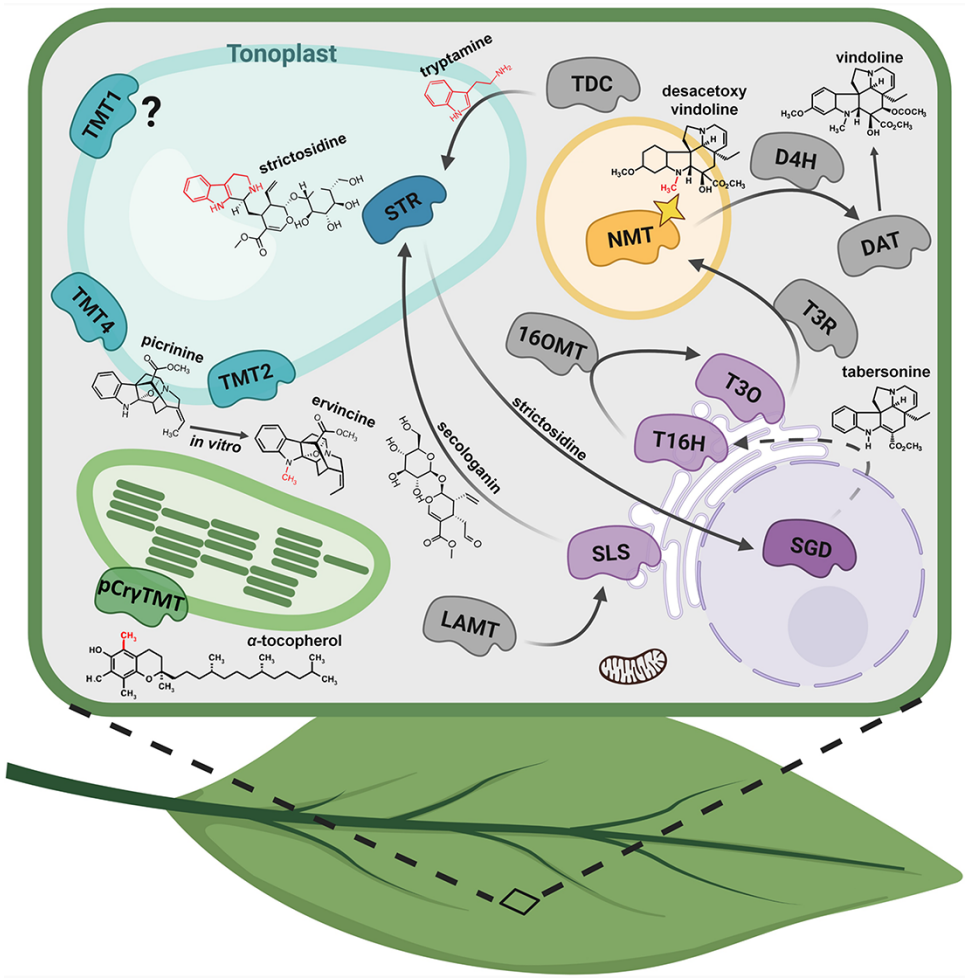

Fig. 11 Schematic illustration of the subcellular organization of *C. roseus* γTMThs and MIA-related enzymes in cells. Enzyme localization is color-coded: green—plastid envelope membrane; light blue—tonoplast; dark blue—vacuole; orange—peroxisome; grey—cytosol; light purple—ER; dark purple—nucleus. The yellow star represents the identified atypical peroxisome targeting sequence (PST1). Grey arrows show pathway enzymatic steps. The dark grey dashed arrow indicates that several enzymatic steps were omitted for scheme simplification. LAMT: loganic acid *O*-methyltransferase; SLS: secologanin synthase; TDC: tryptophan decarboxylase; STR: strictosidine synthase; SGD: strictosidine β-glucosidase; T16H: tabersonine 16-hydroxylase; 16OMT: tabersonine 16-*O*-methyltransferase, T3O: tabersonine 3-oxygenase, T3R: tabersonine 3-reductase, NMT: 16-methoxy-2,3-dihydro-3-hydroxytabersonine *N*-methyltransferase, D4H: deacetoxyvindoline 4-hydroxylase, DAT: deacetylvindoline *O*-acetyltransferase, TMT: γ-tocopherol methyltra–nsferase homolog.

Panchy et al. 2016, Lichman et al. 2020). Genomic clustering of paralogs has been reported for some MIA biosynthetic genes (Kellner et al. 2015, Zhao et al. 2017, Franke et al. 2019, Rai et al. 2021) and, similarly to the three aforementioned NMTs in *C. roseus*, genomic clustering of *O*-methyltransferases involved in flavonoid biosynthesis has been reported in Fabaceae and Lamiaceae species (De Vega et al. 2015, Mochida et al. 2017, Zhao et al. 2019). To support the concept of functional relationship, we conducted enzymatic assays with recombinant enzymes and picrinine as a substrate given that RsPiNMT and CrTMT4 are closely related (**Supplementary Fig. S3**, **Fig. 10**). Through the production of ervincine, these assays specifically revealed that CrTMT2 and CrTMT4 encode functional alkaloid NMTs capable of picrinine methylation. Interestingly, we observed that RsPiNMT, CrTMT2 and CrTMT4 share similar localization and activity. By contrast, CrTMT1 that is not clustered with CrNMT within the genome of *C. roseus* does not display the picrinine NMT activity suggesting a more distant function. Although we used picrinine as a substrate to screen for enzymatic activity among the candidates, this alkaloid is not known to be produced in *C. roseus*. Therefore, our assay only confirmed that CrTMT2 and CrTMT4 are *bona fide* alkaloid NMTs but their roles *in planta* as well as their respective actual substrates remain to be addressed. Most likely these enzymes are involved in *N*-methylation of minor alkaloids that are closely related to the structure of picrinine like vincorine (Jossang et al. 1998) or cathafoline (Rasoanaivo et al. 1973, Jacquier et al. 1980) that has been identified in *C. roseus* and *C. longifolius*, respectively. Other minor *N*-methylated alkaloids identified in *C. roseus* that could potentially be substrates of CrTMT2 and

CrTMT4 include cathovaline (Rahman and Chaudhry 1985) and bannucine (Rahman et al. 1986). The lack of commercial sources and even standards of minor alkaloids hampers the functional characterization of these enzymes. However, reconstitution of biosynthetic pathways in heterologous systems could be an attractive approach to produce tailor-made precursors in high quantities and thus facilitate further functional studies (Carqueijeiro et al. 2020, Courdavault et al. 2020, Guirimand et al. 2021).

In conclusion, we performed an extensive localization study to shed light on the subcellular logistics of alkaloid NMTs leading to the association of tonoplast and peroxisomes to MIA synthesis. Beyond filling a gap into the controversial localization of CrNMT, our analysis also expands our knowledge of the metabolic channeling within the plant cells. In the developing context of natural product engineering in heterologous hosts (Courdavault et al. 2020), such compartments could inspire new metabolic engineering approaches as recently described for yeast peroxisomes (Dusséaux et al. 2020, Kulagina et al. 2021).

Materials and Methods

Plant and cell growth conditions

Seeds of *C. roseus* and *R. serpentina* from our greenhouse were germinated according to Carqueijeiro et al. (2015) and Corbin et al. (2017), respectively. The resulting plants were then grown at 28°C under a 16 h light/8 h dark cycle. *V. minor* leaves and roots were collected in the botanical garden of Tours. All these samples were used for RNA extraction. The *C. roseus* C20A cell suspension culture used for subcellular localization studies was propagated in Gamborg's B5 medium (Duchefa) at 24°C under continuous shaking (100 rpm) for 7 days as described previously (Guirimand et al. 2009).

RNA extraction and reverse-transcription

RNAs were extracted from young leaves and roots of *C. roseus*, *R. serpentina* and *V. minor* using the NucleoSpin RNA Plus Kit (Macherey-Nagel) according to manufacturer's recommendations. First-strand cDNA was synthesized from 0.5 μg of total RNA using oligo(dT)18 primers (0.5 μM) and 15 units of Thermoscript reverse transcriptase (Invitrogen). Following reverse transcription, complementary RNA was removed by treatment with *Escherichia coli* RNase H (Invitrogen) for 20 min at 37°C as described previously (Parage et al. 2016).

Transcriptomic resources and sequence alignment

Identification of γTMT orthologs was achieved by interrogating the consensus *C. roseus* transcriptome CDF97 (Dugé de Bernonville et al. 2015b) (http://bbv-ea2106.sciences.univ-tours.fr/images/files_to_download/BAFC94.fasta) using VTE4 as query. Sequence alignments were performed using Clustal Omega and graphically displayed with BoxShade (https://embnet.vital-it.ch/software/BOX_form.html).

Bioinformatics prediction of subcellular localizations

Whole amino-acid sequences of the putative *C. roseus* γTMTh, VmPiNMT, RsPiNMT, RsANMT, RsNNMT and CrNMT were used for bioinformatics predictions performed using the PSORTII, WolfPSORT, Predotar, ChloroP 1.1 and TargetP 1.1 servers. For all predictions, default 'cut-off' and plant were selected. Prediction of transmembrane helices was conducted with TMHMM (Krogh et al. 2001) and MemBrain (Yin et al. 2017) servers. Prediction of protein post-translational lipid modifications was conducted with GPS-Lipid (Xie et al. 2016).

Constructs for subcellular localization studies

Coding sequences were amplified with the corresponding primers described in **Supplementary Table S1** and the PCR products were digested with *Spe*I. In order to generate constructs fused in frame with YFP at the C-terminal, each product was ligated in a *Spe*I-digested pSCA-YFP plasmid (Guirimand et al. 2009). To generate constructs fused in frame with YFP at the N-terminal, each product was ligated in a *Nhe*I-digested pSCA-YFP plasmid. The subcellular compartment markers have been described in previous publications: plastid-CFP, OEP7-CFP and TIC40-CFP (Guirimand et al. 2020); cytosolic CFP and nucleocytosolic CFP-GUS (Guirimand et al. 2011a), TPK-CFP (Héricourt et al. 2013), STR-CFP (Guirimand et al. 2010a), RFP-AtVSR2 (Shen et al. 2013) and peroxisome (perox)-CFP (Guirimand et al. 2012a).

Biolistic transformation of C. roseus cells and epifluorescence microscopy

Transient transformation of *C. roseus* and onion cells by particle bombardment and fluorescence imaging were performed following the procedures previously described (Guirimand et al. 2009, Foureau et al. 2016, Carqueijeiro et al. 2018b). *C. roseus* or onion cells were bombarded with DNA-coated gold particles (1 μm) and 1,100 psi rupture disc at a stopping-screen-to-target distance of 6 cm, using the Bio-Rad PDS1000/He system and 400 ng of each plasmid per transformation. Cells were cultivated for 16–38 h before being harvested and observed. Cell plasmolysis was performed according to Carqueijeiro et al. (2018b). The subcellular localization was determined using an Olympus BX-51 epifluorescence microscope equipped with an Olympus DP-71 digital camera and a combination of YFP (Chroma#31040, 500–520 nm excitation filter, 540–580 nm band pass emission filter) and CFP (Chroma#31044v2, 426–446 nm excitation filter, 460–500 nm band pass emission filter) filters. Patterns of localization are representative of around 100 observed cells.

Cycloheximide treatment of transiently transformed cells

Transiently transformed cells were treated with cycloheximide (2 μM) for 0 or 4 h prior to observation as described in (Guirimand et al. 2012b).

Production of recombinant C. roseus TMTs in E. coli and enzymatic assays

The coding sequences of CrTMT1, CrTMT2, pCrγTMT, CrTMT4 and CrNMT were amplified with the corresponding primers (**Supplementary Table S1**) and cloned in either pRSET-A (CrTMT1, pCrγTMT and CrNMT) or pQE-30 (CrTMT2 and CrTMT4) expression vectors using the BamHI restriction site. Recombinant protein production was performed in either BL21(DE3) or Top10 *E. coli* strains for pRSET-A and pQE-30 constructs, respectively. Cultures of an $OD_{600} = 0.5$ were induced for 5 h at 28°C with 1 mM isopropyl-β-D-thiogalactopyranoside (IPTG). Protein purification was performed with a Co^{2+} resin (TALON Metal Affinity Resin, Cat. No. 635502, Clontech) according to the manufacturer's instructions. Purified proteins were desalted and dialyzed in 50 mM potassium phosphate buffer pH 7.5 using PD-10 columns (Cat. No. 17085101, GE healthcare). Concentration of proteins was determined by a standard Bradford assay, aliquots in 10% glycerol were flash frozen in liquid nitrogen and stored at −80°C. Enzymatic assays were conducted with 1 μg of purified recombinant proteins in 200 μL activity buffer (100 mM Tris-HCL pH 7.5, 2 mM SAM, 14 mM β-mercaptoethanol and 5 μg picrinine) at 37°C for 120 min under continuous shaking. The reactions were stopped by adding an equal volume of methanol (100%), followed by centrifugation at 16,000 g for 10 min and the supernatants

were analyzed by UPLC-MS. UPLC-MS analyses were performed as described previously (Dugé de Bernonville et al. 2017). Data collection was carried out in selected ion monitoring mode for picrinine (m/z 339; Rt = 11.29) and ervincine (m/z 353; Rt = 13.54).

Supplementary Data

Supplementary data are available at *PCP* online.

Data Availability

The cDNA sequences of the enzymes studied in this article can be accessed in the GenBank database (https://www.ncbi.nlm.nih.gov/genbank/) under accession no. KC708450 (VmPiNMT), KC708448 (RsPiNMT), KC708445 (RsANMT), KC708449 (RsNNMT), HM584929 (CrNMT), MZ367707 (CrTMT1), MZ367708 (CrTMT2), MZ367709 (pCrγTMT), MZ367710 (CrTMT4), AF104220 (AtVTE4; AT1G64970), AY217336 (PsCNMT), DQ028579 (PsTNMT).

Funding

The authors acknowledge funding from the ARD2020 Biopharmaceutical program of the Région Centre Val de Loire (BioPROPHARM, CatharSIS and ETOPOCentre projects), and ANR MIACYC (ANR-20-CE43-0010). GG and VC acknowledge 'le STUDIUM' for a STUDIUM Research Fellowship and STUDIUM Research Consortium grant, respectively.

Acknowledgements

The authors would like to acknowledge Prof. Peter Facchini (University of Calgary) for kindly providing plasmids encompassing the PsCNMT and PsTNMT sequences, Prof. Vincenzo De Luca (Brock University) for kindly providing plasmids encompassing the RsNNMT and RsANMT sequences and Prof. Liwen Jiang (Chinese University of Hong Kong) for kindly providing the RFP-VSR2 marker.

Disclosures

The authors have no conflicts of interest to declare.

References

Abas, L. and Luschnig, C. (2010) Maximum yields of microsomal-type membranes from small amounts of plant material without requiring ultracentrifugation. *Anal. Biochem.* 401: 217–227.

Besseau, S., Kellner, F., Lanoue, A., Thamm, A.M.K., Salim, V., Schneider, B., et al. (2013) A pair of tabersonine 16-hydroxylases initiates the synthesis of vindoline in an organ-dependent manner in *Catharanthus roseus*. *Plant Physiol.* 163: 1792–1803.

Bracha-Drori, K., Shichrur, K., Lubetzky, T.C. and Yalovsky, S. (2008) Functional analysis of *Arabidopsis* postprenylation caax processing enzymes and their function in subcellular protein targeting. *Plant Physiol.* 148: 119–131.

Bréhélin, C., Kessler, F. and van Wijk, K.J. (2007) Plastoglobules: versatile lipoprotein particles in plastids. *Trends Plant Sci.* 12: 260–266.

Caputi, L., Franke, J., Farrow, S.C., Chung, K., Payne, R.M.E., Nguyen, T.-D., et al. (2018) Missing enzymes in the biosynthesis of the anticancer drug vinblastine in Madagascar periwinkle. *Science* 360: 1235–1239.

Carqueijeiro, I., Dugé de Bernonville, T., Lanoue, A., Dang, -T.-T., Teijaro, C.N., Paetz, C., et al. (2018a) A BAHD acyltransferase catalyzing 19-*O*-acetylation of tabersonine derivatives in roots of *Catharanthus roseus* enables combinatorial synthesis of monoterpene indole alkaloids. *Plant J.* 94: 469–484.

Carqueijeiro, I., Langley, C., Grzech, D., Koudounas, K., Papon, N., O'Connor, S.E., et al. (2020) Beyond the semi-synthetic artemisinin: metabolic engineering of plant-derived anti-cancer drugs. *Curr. Opin. Biotechnol.* 65: 17–24.

Carqueijeiro, I., Masini, E., Foureau, E., Sepúlveda, L.J., Marais, E., Lanoue, A., et al. (2015) Virus-induced gene silencing in *Catharanthus roseus* by biolistic inoculation of tobacco rattle virus vectors. *Plant Biol.* 17: 1242–1246.

Carqueijeiro, I., Sepúlveda, L.J., Mosquera, A., Payne, R., Corbin, C., Papon, N., et al. (2018b) Vacuole-targeted proteins: ins and outs of subcellular localization studies. *In* Plant Vacuolar Trafficking: Methods and Protocols. Edited by Pereira, C. pp. 33–54. Springer New York, New York.

Carrie, C., Murcha, M.W., Millar, A.H., Smith, S.M. and Whelan, J. (2007) Nine 3-ketoacyl-CoA thiolases (KATs) and acetoacetyl-CoA thiolases (ACATs) encoded by five genes in *Arabidopsis thaliana* are targeted either to peroxisomes or cytosol but not to mitochondria. *Plant Mol. Biol.* 63: 97–108.

Cázares-Flores, P., Levac, D. and De Luca, V. (2016) *Rauvolfia serpentina N*-methyltransferases involved in ajmaline and N_{β}-methylajmaline biosynthesis belong to a gene family derived from γ-tocopherol *C*-methyltransferase. *Plant J.* 87: 335–342.

Choi, S.C., Lee, S., Kim, S.-R., Lee, Y.-S., Liu, C., Cao, X., et al. (2014) Trithorax group protein *Oryza sativa* Trithorax1 controls flowering time in rice via interaction with Early heading date3. *Plant Physiol.* 164: 1326–1337.

Corbin, C., Lafontaine, F., Sepúlveda, L.J., Carqueijeiro, I., Courtois, M., Lanoue, A., et al. (2017) Virus-induced gene silencing in *Rauwolfia species*. *Protoplasma* 254: 1813–1818.

Costa, M.M.R., Hilliou, F., Duarte, P.C., Pereira, L.S.G., Almeida, I., Leech, M., et al. (2008) Molecular cloning and characterization of a vacuolar class III peroxidase involved in the metabolism of anticancer alkaloids in *Catharanthus roseus*. *Plant Physiol.* 146: 413–417.

Courdavault, V., O'Connor, S.E., Oudin, A., Besseau, S. and Papon, N. (2020) Towards the microbial production of plant-derived anticancer drugs. *Trends Cancer* 6: 444–448.

Courdavault, V., Papon, N., Clastre, M., Giglioli-Guivarc'h, N., St-Pierre, B. and Burlat, V. (2014) A look inside an alkaloid multisite plant: the *Catharanthus* logistics. *Curr. Opin. Plant Biol.* 19: 43–50.

De Luca, V., Balsevich, J., Tyler, R.T. and Kurz, W.G.W. (1987) Characterization of a novel *N*-methyltransferase (NMT) from *Catharanthus roseus* plants. *Plant Cell Rep.* 6: 458–461.

De Luca, V. and Cutler, A.J. (1987) Subcellular localization of enzymes involved in indole alkaloid biosynthesis in *Catharanthus roseus*. *Plant Physiol.* 85: 1099–1102.

De Vega, J.J., Ayling, S., Hegarty, M., Kudrna, D., Goicoechea, J.L., Ergon, Å., et al. (2015) Red clover (*Trifolium pratense* L.) draft genome provides a platform for trait improvement. *Sci. Rep.* 5: 17394.

Dethier, M. and De Luca, V. (1993) Partial purification of an *N*-methyltransferase involved in vindoline biosynthesis in *Catharanthus roseus*. *Phytochemistry* 32: 673–678.

Dugé de Bernonville, T., Carqueijeiro, I., Lanoue, A., Lafontaine, F., Sánchez Bel, P., Liesecke, F., et al. (2017) Folivory elicits a strong defense reaction in *Catharanthus roseus*: metabolomic and transcriptomic analyses reveal distinct local and systemic responses. *Sci. Rep.* 7: 40453.

Dugé de Bernonville, T., Clastre, M., Besseau, S., Oudin, A., Burlat, V., Glévarec, G., et al. (2015a) Phytochemical genomics of the Madagascar periwinkle: unravelling the last twists of the alkaloid engine. *Phytochemistry* 113: 9–23.

Dugé de Bernonville, T., Foureau, E., Parage, C., Lanoue, A., Clastre, M., Londono, M.A., et al. (2015b) Characterization of a second secologanin synthase isoform producing both secologanin and secoxyloganin allows enhanced de novo assembly of a *Catharanthus roseus* transcriptome. *BMC Genom.* 16: 619.

Dusséaux, S., Wajn, W.T., Liu, Y., Ignea, C. and Kampranis, S.C. (2020) Transforming yeast peroxisomes into microfactories for the efficient production of high-value isoprenoids. *Proc. Natl. Acad. Sci.* 117: 31789–31799.

Endler, A., Meyer, S., Schelbert, S., Schneider, T., Weschke, W., Peters, S.W., et al. (2006) Identification of a vacuolar sucrose transporter in barley and *Arabidopsis* mesophyll cells by a tonoplast proteomic approach. *Plant Physiol.* 141: 196–207.

Eubel, H., Lee, C.P., Kuo, J., Meyer, E.H., Taylor, N.L. and Millar, A.H. (2007) Technical advance: free-flow electrophoresis for purification of plant mitochondria by surface charge. *Plant J.* 52: 583–594.

Eubel, H., Meyer, E.H., Taylor, N.L., Bussell, J.D., O'Toole, N., Heazlewood, J.L., et al. (2008) Novel proteins, putative membrane transporters, and an integrated metabolic network are revealed by quantitative proteomic analysis of *Arabidopsis* cell culture peroxisomes. *Plant Physiol.* 148: 1809–1829.

Fornara, V., Onelli, E., Sparvoli, F., Rossoni, M., Aina, R., Marino, G., et al. (2008) Localization of stilbene synthase in *Vitis vinifera* L. During berry development. *Protoplasma* 233: 83–93.

Foureau, E., Carqueijeiro, I., Dugé de Bernonville, T., Melin, C., Lafontaine, F., Besseau, S., et al. (2016) Prequels to synthetic biology: from candidate gene identification and validation to enzyme subcellular localization in plant and yeast cells. *In* Methods in Enzymology. Edited by O'Connor, S.E. pp. 167–206. Academic Press, Cambridge, MA, USA.

Franke, J., Kim, J., Hamilton, J.P., Zhao, D., Pham, G.M., Wiegert-Rininger, K., et al. (2019) Gene discovery in *Gelsemium* highlights conserved gene clusters in monoterpene indole alkaloid biosynthesis. *ChemBioChem* 20: 83–87.

González, B. and Vera, P. (2019) Folate metabolism interferes with plant immunity through 1C methionine synthase-directed genome-wide DNA methylation enhancement. *Mol. Plant* 12: 1227–1242.

Guirimand, G., Burlat, V., Oudin, A., Lanoue, A., St-Pierre, B. and Courdavault, V. (2009) Optimization of the transient transformation of *Catharanthus roseus* cells by particle bombardment and its application to the subcellular localization of hydroxymethylbutenyl 4-diphosphate synthase and geraniol 10-hydroxylase. *Plant Cell Rep.* 28: 1215–1234.

Guirimand, G., Courdavault, V., Lanoue, A., Mahroug, S., Guihur, A., Blanc, N., et al. (2010a) Strictosidine activation in Apocynaceae: towards a "nuclear time bomb"? *BMC Plant Biol.* 10: 182.

Guirimand, G., Courdavault, V., St-Pierre, B. and Burlat, V. (2010b) Biosynthesis and regulation of alkaloids. *In* Plant Developmental Biology - Biotechnological Perspectives: Volume 2. Edited by Pua, E.C. and Davey, M.R. pp. 139–160. Springer Berlin Heidelberg, Berlin, Heidelberg.

Guirimand, G., Guihur, A., Ginis, O., Poutrain, P., Héricourt, F., Oudin, A., et al. (2011a) The subcellular organization of strictosidine biosynthesis in *Catharanthus roseus* epidermis highlights several trans-tonoplast translocations of intermediate metabolites. *FEBS J.* 278: 749–763.

Guirimand, G., Guihur, A., Poutrain, P., Héricourt, F., Mahroug, S., St-Pierre, B., et al. (2011b) Spatial organization of the vindoline biosynthetic pathway in *Catharanthus roseus*. *J. Plant Physiol.* 168: 549–557.

Guirimand, G., Guihur, A., Phillips, M.A., Oudin, A., Glévarec, G., Melin, C., et al. (2012a) A single gene encodes isopentenyl diphosphate isomerase isoforms targeted to plastids, mitochondria and peroxisomes in *Catharanthus roseus*. *Plant Mol. Biol.* 79: 443–459.

Guirimand, G., Simkin, A.J., Papon, N., Besseau, S., Burlat, V., St-Pierre, B., et al. (2012b) Cycloheximide as a tool to investigate protein import in peroxisomes: a case study of the subcellular localization of isoprenoid biosynthetic enzymes. *J. Plant Physiol.* 169: 825–829.

Guirimand, G., Guihur, A., Perello, C., Phillips, M., Mahroug, S., Oudin, A., et al. (2020) Cellular and subcellular compartmentation of the 2*C*-methyl-*D*-erythritol 4-phosphate pathway in the Madagascar periwinkle. *Plants* 9: 462.

Guirimand, G., Kulagina, N., Papon, N., Hasunuma, T. and Courdavault, V. (2021) Innovative tools and strategies for optimizing yeast cell factories. *Trends Biotechnol.* 39: 488–504.

Hagel, J.M. and Facchini, P.J. (2012) Subcellular localization of sanguinarine biosynthetic enzymes in cultured opium poppy cells. *Vitro Cell. Dev. Biol. Plant* 48: 233–240.

Héricourt, F., Chefdor, F., Bertheau, L., Tanigawa, M., Maeda, T., Guirimand, G., et al. (2013) Characterization of histidine-aspartate kinase HK1 and identification of histidine phosphotransfer proteins as potential partners in a *Populus* multistep phosphorelay. *Physiol. Plant.* 149: 188–199.

Hugueney, P., Provenzano, S., Verriès, C., Ferrandino, A., Meudec, E., Batelli, G., et al. (2009) A novel cation-dependent *O*-methyltransferase involved in anthocyanin methylation in grapevine. *Plant Physiol.* 150: 2057–2070.

Jacquier, M.J., Vercauteren, J., Massiot, G., Le Men-Olivier, L., Pussett, J. and Sevenet, T. (1980) Alkaloids of *Alstonia plumosa*. *Phytochemistry* 21: 2973–2977.

Jo, Y. and Hyun, T.K. (2011) Genome-wide identification of antioxidant component biosynthetic enzymes: comprehensive analysis of ascorbic acid and tocochromanols biosynthetic genes in rice. *Comput. Biol. Chem.* 35: 261–268.

Jossang, A., Fodor, P. and Bodo, B. (1998) A new structural class of bisindole alkaloids from the seeds of *Catharanthus roseus*: vingramine and methylvingramine. *J. Org. Chem.* 63: 7162–7167.

Jung, C., Lee, G.-J., Jang, M., Lee, M., Lee, J., Kang, H., et al. (2011) Identification of sorting motifs of AtβFruct4 for trafficking from the ER to the vacuole through the Golgi and PVC. *Traffic* 12: 1774–1792.

Kellner, F., Kim, J., Clavijo, B.J., Hamilton, J.P., Childs, K.L., Vaillancourt, B., et al. (2015) Genome-guided investigation of plant natural product biosynthesis. *Plant J.* 82: 680–692.

Koch, M., Lemke, R., Heise, K.-P. and Mock, H.-P. (2003) Characterization of γ-tocopherol methyltransferases from *Capsicum annuum* L and *Arabidopsis thaliana*. *Eur. J. Biochem.* 270: 84–92.

Kodama, Y., Shinya, T. and Sano, H. (2008) Dimerization of *N*-methyltransferases involved in caffeine biosynthesis. *Biochimie* 90: 547–551.

Krogh, A., Larsson, B., von Heijne, G. and Sonnhammer, E.L.L. (2001) Predicting transmembrane protein topology with a hidden Markov model: application to complete genomes. *J. Mol. Biol.* 305: 567–580.

Kulagina, N., Besseau, S., Papon, N. and Courdavault, V. (2021) Peroxisomes: a new hub for metabolic engineering in yeast. *Front. Bioeng. Biotechnol.* 9: 659431.

Lee, C., Teng, Q., Zhong, R., Yuan, Y., Haghighat, M. and Ye, Z.-H. (2012) Three arabidopsis DUF579 domain-containing GXM proteins are methyltransferases catalyzing 4-*O*-methylation of glucuronic acid on xylan. *Plant Cell Physiol.* 53: 1934–1949.

Levac, D., Cázares, P., Yu, F. and De Luca, V. (2016) A picrinine *N*-methyltransferase belongs to a new family of γ-tocopherol-like methyltransferases found in medicinal plants that make biologically active monoterpenoid indole alkaloids. *Plant Physiol.* 170: 1935–1944.

Lichman, B.R., Godden, G.T. and Buell, C.R. (2020) Gene and genome duplications in the evolution of chemodiversity: perspectives from studies of Lamiaceae. *Curr. Opin. Plant Biol.* 55: 74–83.

Liscombe, D.K., Usera, A.R. and O'Connor, S.E. (2010) Homolog of tocopherol *C* methyltransferases catalyzes *N* methylation in anticancer alkaloid biosynthesis. *Proc. Natl. Acad. Sci.* 107: 18793–18798.

Madyastha, K.M., Ridgway, J.E., Dwyer, J.G. and Coscia, C.J. (1977) Subcellular localization of a cytochrome P-450-dependent monogenase in vesicles of the higher plant *Catharanthus roseus*. *J. Cell Biol.* 72: 302–313.

Magnani, R., Nayak, N.R., Mazarei, M., Dirk, L.M.A. and Houtz, R.L. (2007) Polypeptide substrate specificity of *Ps*LSMT: a set domain protein methyltransferase. *J. Biol. Chem.* 282: 27857–27864.

Miettinen, K., Dong, L., Navrot, N., Schneider, T., Burlat, V., Pollier, J., et al. (2014) The seco-iridoid pathway from *Catharanthus roseus*. *Nat. Commun.* 5: 3606.

Mochida, K., Sakurai, T., Seki, H., Yoshida, T., Takahagi, K., Sawai, S., et al. (2017) Draft genome assembly and annotation of *Glycyrrhiza uralensis*, a medicinal legume. *Plant J.* 89: 181–194.

Moore, R.C. and Purugganan, M.D. (2005) The evolutionary dynamics of plant duplicate genes. *Curr. Opin. Plant Biol.* 8: 122–128.

Morris, J.S. and Facchini, P.J. (2019) Molecular origins of functional diversity in benzylisoquinoline alkaloid methyltransferases. *Front. Plant Sci.* 10: 1058.

Muñoz, P. and Munné-Bosch, S. (2019) Vitamin E in plants: biosynthesis, transport, and function. *Trends Plant Sci.* 24: 1040–1051.

Naconsie, M., Kato, K., Shoji, T. and Hashimoto, T. (2014) Molecular evolution of *N*-methylputrescine oxidase in tobacco. *Plant Cell Physiol.* 55: 436–444.

Nakayama, T., Takahashi, S. and Waki, T. (2019) Formation of flavonoid metabolons: functional significance of protein-protein interactions and impact on flavonoid chemodiversity. *Front. Plant Sci.* 10: 821.

Nozoye, T., Nagasaka, S., Bashir, K., Takahashi, M., Kobayashi, T., Nakanishi, H., et al. (2014) Nicotianamine synthase 2 localizes to the vesicles of iron-deficient rice roots, and its mutation in the YXXφ or LL motif causes the disruption of vesicle formation or movement in rice. *Plant J.* 77: 246–260.

Nützmann, H.-W., Huang, A. and Osbourn, A. (2016) Plant metabolic clusters – from genetics to genomics. *New Phytolo.* 211: 771–789.

O'Connor, S.E. and Maresh, J.J. (2006) Chemistry and biology of monoterpene indole alkaloid biosynthesis. *Nat. Prod. Rep.* 23: 532–547.

Pan, R., Reumann, S., Lisik, P., Tietz, S., Olsen, L.J. and Hu, J. (2018) Proteome analysis of peroxisomes from dark-treated senescent *Arabidopsis* leaves. *J. Integr. Plant Biol.* 60: 1028–1050.

Panchy, N., Lehti-Shiu, M. and Shiu, S.-H. (2016) Evolution of gene duplication in plants. *Plant Physiol.* 171: 2294–2316.

Parage, C., Foureau, E., Kellner, F., Burlat, V., Mahroug, S., Lanoue, A., et al. (2016) Class II cytochrome P450 reductase governs the biosynthesis of alkaloids. *Plant Physiol.* 172: 1563–1577.

Payne, R.M.E., Xu, D., Foureau, E., Teto Carqueijeiro, M.I.S., Oudin, A., Bernonville, T.D.D., et al. (2017) An NPF transporter exports a central monoterpene indole alkaloid intermediate from the vacuole. *Nat. Plants* 3: 16208.

Pedrazzini, E., Komarova, N.Y., Rentsch, D. and Vitale, A. (2013) Traffic routes and signals for the tonoplast. *Traffic* 14: 622–628.

Pracharoenwattana, I., Cornah, J.E. and Smith, S.M. (2005) *Arabidopsis* peroxisomal citrate synthase is required for fatty acid respiration and seed germination. *Plant Cell* 17: 2037–2048.

Quan, S., Yang, P., Cassin-Ross, G., Kaur, N., Switzenberg, R., Aung, K., et al. (2013) Proteome analysis of peroxisomes from etiolated *Arabidopsis* seedlings identifies a peroxisomal protease involved in β-oxidation and development. *Plant Physiol.* 163: 1518–1538.

Rahman, A., Ali, I. and Chaudhry, M.I. (1985) Isolation and 13c-nmr studies on cathovaline, an alkaloid from the leaves of *Catharanthus roseus*. *Planta Med.* 51: 447–448.

Rahman, A., Ali, I. and Chaudhary, M.I. (1986) Bannucine – a new dihydroindole alkaloid from *Catharanthus roseus* (L.) G. Don. *J. Chem. Soc. Perkin Trans.* 1: 923–926.

Rai, A., Hirakawa, H., Nakabayashi, R., Kikuchi, S., Hayashi, K., Rai, M., et al. (2021) Chromosome-level genome assembly of *Ophiorrhiza pumila* reveals the evolution of camptothecin biosynthesis. *Nat. Commun.* 12: 405.

Rasoanaivo, P., Langlois, N., Potier, P. and Bladon, P. (1973) Plantes malgaches x (1) - nouvel alcaloide du *Catharanthus longifolius* Pich. (Apocynacees). *Tetrahedron Lett.* 14: 1425–1428.

Ravanel, S., Block, M.A., Rippert, P., Jabrin, S., Curien, G., Rébeillé, F., et al. (2004) Methionine metabolism in plants: chloroplasts are autonomous for *de novo* methionine synthesis and can import *S*-adenosylmethionine from the cytosol. *J. Biol. Chem.* 279: 22548–22557.

Reumann, S., Babujee, L., Ma, C., Wienkoop, S., Siemsen, T., Antonicelli, G.E., et al. (2007) Proteome analysis of *Arabidopsis* leaf peroxisomes reveals novel targeting peptides, metabolic pathways, and defense mechanisms. *Plant Cell* 19: 3170–3193.

Reumann, S., Chowdhary, G. and Lingner, T. (2016) Characterization, prediction and evolution of plant peroxisomal targeting signals type 1 (PTS1s). *Biochim. Biophys. Acta Mol. Cell Res.* 1863: 790–803.

Rueffer, M., Amann, M. and Zenk, M.H. (1986) S-Adenosyl-L-methionine: columbamine-*O*-methyl transferase, a compartmentalized enzyme in protoberberine biosynthesis. *Plant Cell Rep.* 5: 182–185.

Saslowsky, D. and Winkel-Shirley, B. (2001) Localization of flavonoid enzymes in *Arabidopsis* roots. *Plant J.* 27: 37–48.

Segami, S., Makino, S., Miyake, A., Asaoka, M. and Maeshima, M. (2014) Dynamics of vacuoles and H^+-pyrophosphatase visualized by monomeric green fluorescent protein in *Arabidopsis*: artifactual bulbs and native intravacuolar spherical structures. *Plant Cell* 26: 3416–3434.

Shaipulah, N.F.M., Muhlemann, J.K., Woodworth, B.D., Van Moerkercke, A., Verdonk, J.C., Ramirez, A.A., et al. (2016) *CCoAOMT* down-regulation activates anthocyanin biosynthesis in petunia. *Plant Physiol.* 170: 717–731.

Shen, H., He, Z., Yan, H., Xing, Z., Chen, Y., Xu, W., et al. (2014) The fronds tonoplast quantitative proteomic analysis in arsenic hyperaccumulator *Pteris vittata* L. *J. Proteomics* 105: 46–57.

Shen, J., Suen, P.K., Wang, X., Lin, Y., Lo, S.W., Rojo, E., et al. (2013) An *in vivo* expression system for the identification of cargo proteins of vacuolar sorting receptors in *Arabidopsis* culture cells. *Plant J.* 75: 1003–1017.

Shintani, D. and DellaPenna, D. (1998) Elevating the vitamin E content of plants through metabolic engineering. *Science* 282: 2098–2100.

Simkin, A.J., Guirimand, G., Papon, N., Courdavault, V., Thabet, I., Ginis, O., et al. (2011) Peroxisomal localisation of the final steps of the mevalonic acid pathway. *In Planta. Planta* 234: 903.

Simkin, A.J., Miettinen, K., Claudel, P., Burlat, V., Guirimand, G., Courdavault, V., et al. (2013) Characterization of the plastidial geraniol synthase from Madagascar periwinkle which initiates the monoterpenoid branch of the alkaloid pathway in internal phloem associated parenchyma. *Phytochemistry* 85: 36–43.

Soll, J., Schultz, G., Joyard, J., Douce, R. and Block, M.A. (1985) Localization and synthesis of prenylquinones in isolated outer and inner envelope

membranes from spinach chloroplasts. *Arch. Biochem. Biophys.* 238: 290–299.

Stavrinides, A., Tatsis, E.C., Caputi, L., Foureau, E., Stevenson, C.E.M., Lawson, D.M., et al. (2016) Structural investigation of heteroyohimbine alkaloid synthesis reveals active site elements that control stereoselectivity. *Nat. Commun.* 7: 12116.

Stavrinides, A., Tatsis, E.C., Foureau, E., Caputi, L., Kellner, F., Courdavault, V., et al. (2015) Unlocking the diversity of alkaloids in *Catharanthus roseus*: nuclear localization suggests metabolic channeling in secondary metabolism. *Chem. Biol.* 22: 336–341.

St-Pierre, B., Besseau, S., Clastre, M., Courdavault, V., Courtois, M., Crèche, J., et al. (2013) Deciphering the evolution, cell biology and regulation of monoterpene indole alkaloids. *In* Advances in Botanical Research. Edited by Giglioli-Guivarc'h, N. pp. 73–109. Academic Press, Burlington.

Tamiru, M., Takagi, H., Abe, A., Yokota, T., Kanzaki, H., Okamoto, H., et al. (2016) A chloroplast-localized protein lesion and lamina bending affects defence and growth responses in rice. *New Phytolo.* 210: 1282–1297.

Tanabe, Y., Maruyama, J.-I., Yamaoka, S., Yahagi, D., Matsuo, I., Tsutsumi, N., et al. (2011) Peroxisomes are involved in biotin biosynthesis in *Aspergillus* and *Arabidopsis*. *J. Biol. Chem.* 286: 30455–30461.

Tang, R.-J., Liu, H., Yang, Y., Yang, L., Gao, X.-S., Garcia, V.J., et al. (2012) Tonoplast calcium sensors CBL2 and CBL3 control plant growth and ion homeostasis through regulating V-ATPase activity in *Arabidopsis*. *Cell Res.* 22: 1650–1665.

Teng, J., Yan, C., Zeng, W., Zhang, Y., Zeng, Z. and Huang, Y. (2020) Purification and characterization of theobromine synthase in a theobromine-enriched wild tea plant (*Camellia gymnogyna* Chang) from Dayao Mountain, China. *Food Chem.* 311: 125875.

Thabet, I., Guirimand, G., Courdavault, V., Papon, N., Godet, S., Dutilleul, C., et al. (2011) The subcellular localization of periwinkle farnesyl diphosphate synthase provides insight into the role of peroxisome in isoprenoid biosynthesis. *J. Plant Physiol.* 168: 2110–2116.

Thabet, I., Guirimand, G., Guihur, A., Lanoue, A., Courdavault, V., Papon, N., et al. (2012) Characterization and subcellular localization of geranylgeranyl diphosphate synthase from *Catharanthus roseus*. *Mol. Biol. Rep.* 39: 3235–3243.

Toda, K., Kuroiwa, H., Senthil, K., Shimada, N., Aoki, T., Ayabe, S.-I., et al. (2012) The soybean F3′H protein is localized to the tonoplast in the seed coat hilum. *Planta* 236: 79–89.

Wojcik, S. and Kriechbaumer, V. (2021) Go your own way: membrane-targeting sequences. *Plant Physiol.* 185: 608–618.

Xie, Y., Zheng, Y., Li, H., Luo, X., He, Z., Cao, S., et al. (2016) GPS-Lipid: a robust tool for the prediction of multiple lipid modification sites. *Sci. Rep.* 6: 28249.

Yin, X., Yang, J., Xiao, F., Yang, Y. and Shen, H.-B. (2017) MemBrain: an easy-to-use online webserver for transmembrane protein structure prediction. *Nano-Micro Lett.* 10: 2.

Zbierzak, A.M., Kanwischer, M., Wille, C., Vidi, P.-A., Giavalisco, P., Lohmann, A., et al. (2009) Intersection of the tocopherol and plastoquinol metabolic pathways at the plastoglobule. *Biochem. J.* 425: 389–399.

Zhao, D., Hamilton, J.P., Pham, G.M., Crisovan, E., Wiegert-Rininger, K., Vaillancourt, B., et al. (2017) *De novo* genome assembly of *Camptotheca acuminata*, a natural source of the anti-cancer compound camptothecin. *GigaScience* 6: 1–7.

Zhao, Q., Yang, J., Cui, M.-Y., Liu, J., Fang, Y., Yan, M., et al. (2019) The reference genome sequence of *Scutellaria baicalensis* provides insights into the evolution of wogonin biosynthesis. *Mol Plant* 12: 935–950.